(2)

222300-1-F

Final Report

ARGUS/LLNL IR CAMERA CALIBRATION AND CHARACTERIZATION

D.J. WITTE

NOVEMBER 1989

USAF Weapons Laboratory/
Advanced Radiation Office
WL/ARCG
Kirtland AFB, NM 87117-6008

ERIM P.O. Box 8618
Ann Arbor, MI 48107-8618

REPORT DOCUMENTATION PAGE

Form Approved
OMB No. 0704-0188

1a REPORT SECURITY CLASSIFICATION Unclassified	1b RESTRICTIVE MARKINGS
2a SECURITY CLASSIFICATION AUTHORITY	3 DISTRIBUTION/AVAILABILITY OF REPORT
2b DECLASSIFICATION/DOWNGRADING SCHEDULE	
4 PERFORMING ORGANIZATION REPORT NUMBERS(S) 222300-1-F	5 MONITORING ORGANIZATION REPORT NUMBER(S)
6a NAME OF PERFORMING ORGANIZATION ERIM 6b OFFICE SYMBOL *(if applicable)*	7a NAME OF MONITORING ORGANIZATION
6c ADDRESS (City, State, and ZIP Code) P. O. Box 8618 Ann Arbor, MI 48107	7b ADDRESS (City, State, and ZIP Code)
8a NAME OF FUNDING /SPONSORING ORGANIZATION USAF WL/AR 8b OFFICE SYMBOL *(if applicable)*	9 PROCUREMENT INSTRUMENT IDENTIFICATION NUMBER
8c ADDRESS (City, State, and ZIP Code) WL/ARCG Kirtland AFB, NM 87117-6008	10 SOURCE OF FUNDING NUMBERS PROGRAM ELEMENT NO / PROJECT NO / TASK NO / WORK UNIT ACCESSION NO

11 TITLE (Include Security Classification)

ARGUS/LLNL IR Camera Calibration and Characterization (Unclassified)

12 PERSONAL AUTHOR(S)

David J. Witte

13a TYPE OF REPORT	13b TIME COVERED	14 DATE OF REPORT (Year, Month, Day)	15 PAGE COUNT
Final	FROM Oct89 TO Nov89	November 1989	66 + x

16 SUPPLEMENTARY NOTATION

The WL/AR Technical Monitor was Lt. Karl Eager, USAF, Kirtland AFB.
The Principal Investigator was Mr. David Witte, ERIM

17 COSATI CODES			18 SUBJECT TERMS *(Continue on reverse if necessary and identify by block number)*
FIELD	GROUP	SUB-GROUP	Infrared, Radiometry, Calibration, Thermal imaging, Focal plane array, Platinum silicide, ARGUS

19 ABSTRACT *(Continue on reverse if necessary and identify by block number)*

The ARGUS/LLNL IR Camera (aka the ARGUS IR Imaging System) was subjected to a series of laboratory measurements. These measurements were made to define:
(1) The sensor's radiometric transfer function (i.e., calibration curve);
(2) The sensor's radiometric sensitivity;
(3) The sensor's spatial resolution;
(4) The effects of cooling the sensor telescope upon system performance.

The test procedures and test results from the measurements made to define the above items are presented in this report.

20 DISTRIBUTION/AVAILABILITY OF ABSTRACT	21 ABSTRACT SECURITY CLASSIFICATION
☒ UNCLASSIFIED/UNLIMITED ☐ SAME AS RPT ☐ DTIC USERS	Unclassified
22a NAME OF RESPONSIBLE INDIVIDUAL	22b TELEPHONE (Include Area Code) / 22c OFFICE SYMBOL

EXECUTIVE SUMMARY

This report contains the results and description of a laboratory characterization and calibration performed on the ARGUS InfraRed Imaging System (IRI). ARGUS is a USAF aircraft (modified NC-135) that serves as a platform for a variety of optical imaging sensors. These sensors collect data on a variety of targets, including reentry vehicles, objects in low earth orbit, missile plumes, and other aircraft. The IRI is a mid-wave infrared (MWIR) sensor used to collect radiometrically calibratable image data on targets. Recently, some questions have arisen regarding the instrument's performance characteristics and calibration. Consequently, the characterization effort described in this report was undertaken. The specific objectives of this effort were the following:

1. Define calibration curves/equations that relate sensor output signal level to received irradiance.
2. Determine the system radiometric sensitivity--specifically, the Noise Equivalent Spectral Radiance (NESR) in each of the sensor's four spectral bands.
3. Determine the sensor's spatial resolution and assess whether or not the fixed-focus telescope is focussed at infinity.

During the course of the laboratory tests, an additional objective was defined:

4. Assess the change in sensor performance due to cooling the entire camera assembly.

The four test objectives were met. Signal transfer functions were measured using a calibrated, temperature-controllable blackbody source. A procedure for radiometric calibration of data collected with the IR Camera was defined and appears in Appendix B. The Noise Equivalent Radiance (Watts/cm**2/sr) of the sensor at the broadband filter setting, as well as the Noise Equivalent Spectral Radiances (Watts/cm**2/sr/um) for each of the sub-bands, were found to be of the order of 1.E-5 or larger.

The sensor telescope was found to be focussed at an object distance of roughly 1700 feet instead of the specified focus at infinity. Severe mis-focus occurs on objects that are effectively at infinity, e.g., mission targets. Proper alignment of the telescope is therefore required before the next sensor deployment against mission targets. For focussed imagery, the effective horizontal spatial resolution of the system, as defined by its line-spread function, was found to be roughly 75 to 100 microradians.

Tests were made in which the sensor head was cooled. These tests

showed that when the telescope temperature is near 300 Kelvin, the rotating filter wheel cannot be used to gather useful near-simultaneous data in the four spectral bands. The reason for this limitation has to do with the effects of telescope thermal emission upon the Reference Frame correction applied to the sensor's output. The cooled sensor test showed that if the telescope is cooled to approximately 275 K or lower, data collection with the rotating filter wheel can be performed sucessfully.

Recommendations to improve sensor performance were made. These included:

1. Analysis of Electronics Noise Contribution
2. System Spectral Response Characterization
3. Assessment of Random DC Drift
4. Digitally-Based Calibration
5. Cooled Telescope
6. Obtain a New Telescope
7. Direct Digital Recording

These recommendations are discussed in Section 3.2.

TABLE OF CONTENTS

	Page
1.0 INTRODUCTION AND OVERVIEW	1
1.1 Introduction	1
1.2 Sensor Description	2
1.3 Laboratory Equipment Configuration	3
1.4 Calculation of Radiometric Quantities	5
2.0 CHARACTERIZATION TEST RESULTS	9
2.1 Black Level Response Test	9
2.2 Broadband Signal Transfer Test	17
2.3 Spectral Sub-Bands Signal Transfer Test	30
2.4 Noise/Sensitivity Characterization	35
2.5 Cold Sensor Test	45
2.6 Resolution/Focus Test	48
3.0 SUMMARY AND RECOMMENDATIONS	53
3.1 Summary of Test Results	53
3.2 Recommendations for Sensor Improvements	54
Appendix A: RAW LABORATORY TEST DATA	57
Appendix B: CALIBRATION PROCEDURE FOR CORRECTED VIDEO DATA	65

LIST OF FIGURES

		Page
Figure 1-1.	Laboratory Equipment Configuration	4
Figure 1-2.	Atmospheric Spectral Transmission in Lab	7
Figure 2-1.	Ref. Frame Voltage vs. Black Level - Full Range	10
Figure 2-2.	Ref. Frame Voltage vs. Black Level	12
Figure 2-3.	Ref. Frame Voltage vs. Black Level	13
Figure 2-4.	Blank Line Voltage vs. Black Level	15
Figure 2-5.	FG-100 Digital Value vs. Video Signal Level	16
Figure 2-6.	Summary of Broadband Signal Transfer Results	18
Figure 2-7.	IR Imaging System Calibration - Gain = 1X	20
Figure 2-8.	IR Imaging System Calibration - Gain = 2X	21
Figure 2-9.	IR Imaging System Calibration - Gain = 4X	22
Figure 2-10.	IR Imaging System Calibration - Gain = 8X	23
Figure 2-11.	Deviation from Linearity vs. Irradiance	24
Figure 2-12.	IR Imaging System Calibration - Gain = 1X	25
Figure 2-13.	IR Imaging System Calibration - Gain = 2X	26
Figure 2-14.	IR Imaging System Calibration - Gain = 4X	27
Figure 2-15.	IR Imaging System Calibration - Gain = 8X	28
Figure 2-16.	Signal Transfer Results - Red Band (2.04 um)	32
Figure 2-17.	Signal Transfer Results - Blue Band (2.805 um)	33
Figure 2-18.	Signal Transfer Results - Yellow Band (4.484 um)	34
Figure 2-19.	Measured Noise Level vs. Irradiance	39
Figure 2-20.	Normalized RMS Deviation vs. Irradiance	41
Figure 2-21.	Noise Level vs. Frame Integration	43
Figure 2-22.	Line Spread Function Measurements	51

LIST OF TABLES

		Page
Table 2-1.	Black Level Responsivities	11
Table 2-2.	Gain-Specific Values for Black Level Correction	14
Table 2-3.	Measured Broadband Responsivities	29
Table 2-4.	Relative Gain Levels from Broadband Responsivities	29
Table 2-5.	Summary of Bandpass Filter Characteristics	30
Table 2-6.	Sub-Band Responsivity	36
Table 2-7.	Spectral Response Ratios	36
Table 2-8.	Summary of Temporal Noise Measurements	42
Table 2-9.	Summary of IR Camera Sensitivity Measures	44
Table 2-10.	Lens Cap Signals for Cooled and Ambient Telescope	47
Table 2-11.	Summary of Line Spread Measurements	52
Table A-1.	Black Level Response Test Data	58
Table A-2.	Broadband Signal Transfer Test Data	59
Table A-3.	Spectral Sub-Bands Signal Transfer Test Data	61
Table A-4.	RMS Noise Level vs. Irradiance Data	62
Table A-5.	Variance vs. Frame Integration Data	63

1.0 INTRODUCTION AND OVERVIEW

1.1 INTRODUCTION

This report contains the results and description of a laboratory characterization and calibration performed on the ARGUS InfraRed Imaging System (IRI), also known as the IR Camera. The laboratory tests were performed in October 1989 at the Environmental Research Institute of Michigan (ERIM) in Ann Arbor, Michigan.

ARGUS is a USAF aircraft (modified NC-135) that serves as a platform for a variety of optical imaging sensors. These sensors collect data on a variety of targets, including reentry vehicles, objects in low earth orbit, missile plumes, and other aircraft. The IRI is a mid-wave infrared (MWIR) sensor used to collect radiometrically calibratable image data on targets. Recently, some questions have arisen regarding the instrument's performance characteristics and calibration. Consequently, the characterization effort described in this report was undertaken. The specific objectives of this effort were the following:

1. Define calibration curves/equations that relate sensor output signal level to received irradiance.

2. Determine the system radiometric sensitivity--specifically, the Noise Equivalent Spectral Radiance (NESR) in each of the sensor's four spectral bands.

3. Determine the sensor spatial resolution and assess whether or not the fixed-focus telescope is focussed at infinity.

During the course of the laboratory tests, an additional objective was defined, namely, assess the change in sensor performance due to cooling the entire camera assembly.

In order to fulfill the above objectives, six laboratory test sequences were defined and conducted:

1. Black Level Response Test

2. Broadband Signal Transfer Test

3. Spectral Sub-Bands Signal Transfer Test

4. Noise/Sensitivity Characterization

5. Cold Sensor Test

6. Resolution/Focus Test

The purpose, description, and results of each test are presented in Section 2.0. The raw data collected during the tests is provided in Appendix A, unless reported directly in Section 2.0. A procedure for calibration of mission data based on the lab test results appears as Appendix B. The remainder of this section contains a brief description of the sensor's operation, a description of the laboratory configuration employed for the tests, and a discussion of how quantitative radiometric values were defined for the calibration. Section 3.0 presents a summary assessment and recommendations for possible improvements in overall system performance.

1.2 SENSOR DESCRIPTION

The sensor system is composed of two primary components: the camera unit and the signal processing electronics unit. The camera unit consists of a reflective telescope (f/10 Cassegrain with 20 cm aperture; 7.3 cm central obscuration) mated to a detector/dewar assembly. The latter contains a platinum silicide focal plane array (PtSi FPA), measuring 244 elements vertically by 160 elements horizontally. The array subtends a total field of view (FOV) of approximately 0.27 deg. vertically V by 0.36 deg. horizontally. Each detector element measures 40 micrometers (um) vert. by 80 um horiz., and geometrically subtends a instantaneous field of view (IFOV) of 20 microradians (urad) by 40 urad. The active area of each pixel is 25 um by 50 um, which corresponds to a 39% fill factor.

The array is cooled with liquid nitrogen to an operating temperature of approximately 77 Kelvin. It is mounted within an f/1.6 cold-shield that contains both a sapphire window and a 50% transmission neutral density (ND) filter. The presumed purpose of the ND filter is to limit detector saturation resulting from the large amount of internal telescope emission seen by the FPA. The combination of the telescope and cold-shield f-numbers is such that over 97% of the (uncooled) solid angle seen by the detector consists of internal sensor emission.

Located between the telescope and cold-shield assembly is a four-position filter wheel. One of the four positions is unoccupied and allows data collection over the entire bandpass of the detector (nominally, 1.1 - 5.6 um). The remaining three positions contain spectral filters that permit data collection within three narrow sub-bands. Referred to as the Red, Blue, and Yellow bands, these bands are centered at 2.04 um, 2.805 um, and 4.484 um, respectively. The filter wheel can be stopped at any of the four positions, permitting continuous collection within the associated spectral bandpass. Alternatively, the filter may be motor-driven to automatically cycle through the four positions, stopping at each for approximately one second, and completing a full revolution once every seven seconds.

The signal processing electronics unit creates RS-170 standard video output (i.e., 525 line, 30 Hz frames) from the raw detector signals. Each frame consists of two interlaced video fields. A field, consisting of 262.5 video lines (240 active lines), is produced

by reading out alternate detector rows, i.e., 122 of the 244 rows, once every 1/60 second. The even-numbered detector rows, beginning with row zero, are read out in one field; the odd-numbered rows are read out in the next. The two consecutive fields are interlaced to produce the full 525 line (480 active lines) frame. Only alternate "active" lines in any field actually contain video information; the other lines are blank. The result of interlacing two such fields is a frame in which 50% of the "active" lines are blank; however, the pattern formed is "two ON, two OFF," and so has a periodicity of four lines. The two adjacent ON lines represent detector video information from the two separate fields, are thus are separated in time of collection by 1/60 second. This may result in significant motion smear in a frame if there is rapid relative motion between the sensor and target.

Two separate video outputs are produced by the signal processing unit. The two are referred to as the "Corrected" and the "Uncorrected" video outputs. The essential differences between the two are that: (1) a pixel-by-pixel offset correction is applied to the Corrected video; (2) four discrete, operator-selectable gain levels (i.e., relative gains of 1X, 2X, 4X, and 8X) are available with the Corrected video; and (3) a "Black Level" control, which supplies an operator-adjustable bias voltage to the entire active video, is available with the Corrected video. In contrast, no offset correction or variable bias is applied to the Uncorrected video, which is fixed at a gain level roughly equal to that of the Corrected Video 1X setting.

The offset correction used with the Corrected video consists of subtracting (via analog circuitry) a digitally-stored Reference Frame from every frame of data. The Reference Frame itself must be stored every time the system is powered up. During data collection missions, the Reference Frame is typically captured while the sensor views an area of cold, clear sky. Radiometrically, a very cold reference scene is desirable because the absolute signal level of the reference scene is subtracted from all subsequent target data. From the standpoint of calibration, it is therefore necessary to know the radiance (or irradiance) of the reference scene, so that it may be added back into the measured target values. A sufficiently cold reference scene, e.g., the clear sky above 40,000 ft altitude, may be considered to have effectively zero radiant energy within the spectral passband of the sensor, and so may be ignored.

1.3 LABORATORY EQUIPMENT CONFIGURATION

The basic laboratory set-up used for the characterization tests is illustrated in Figure 1-1. A reflective collimator (14 inch diameter, focal length = 100.25 inches) was used to provide plane-wave illumination to the telescope from a blackbody or other target. During data collection missions, the sensor views the target through a germanium window mounted in the aircraft wall. This window was not available for the laboratory tests. Its transmission characteristics have been independently measured, however, and thus, its effects on

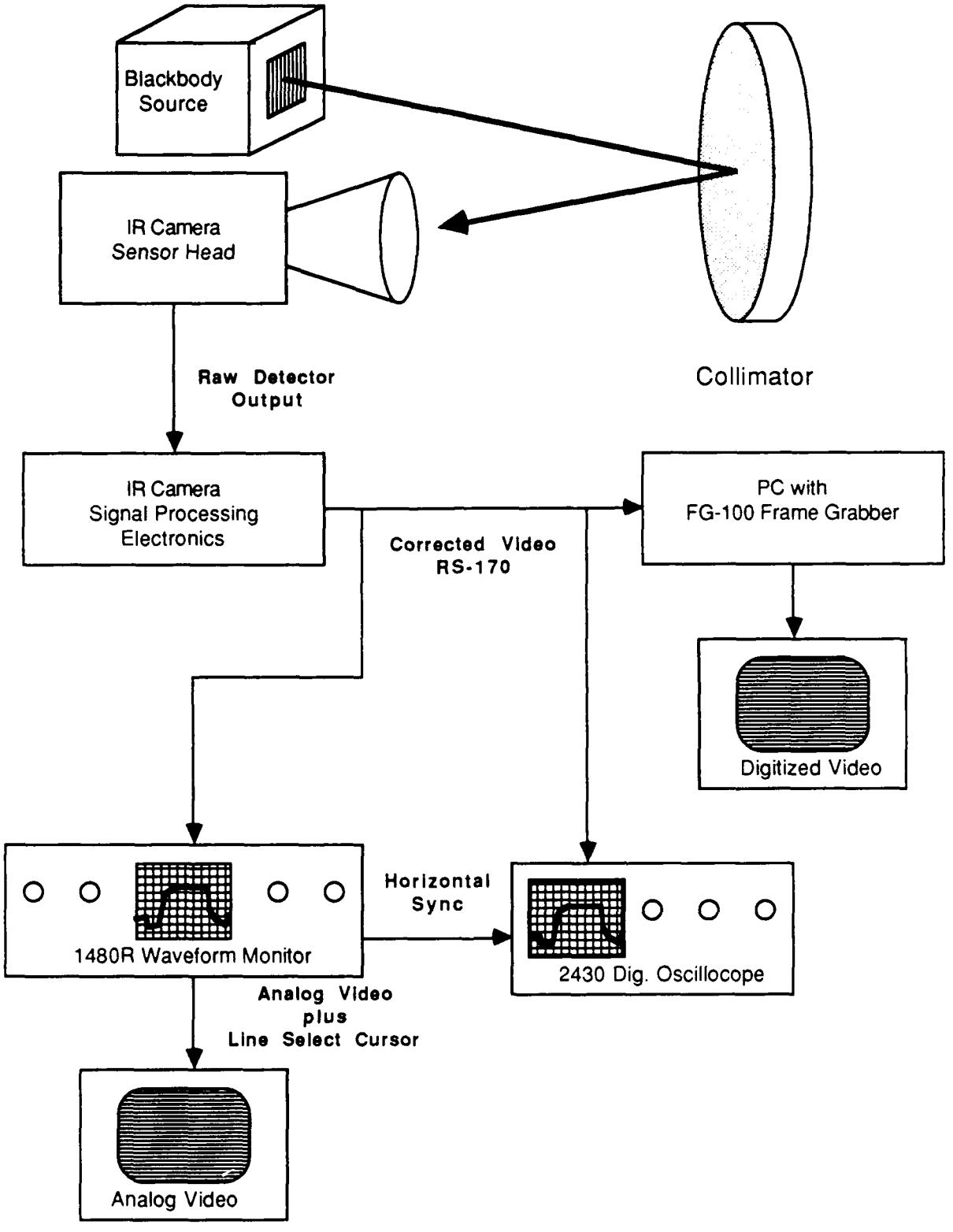

Figure 1-1. Laboratory Equipment Configuration

the system calbration can be accounted for analytically. The procedure for doing so is described in Appendix B.

As shown in Figure 1-1, the Corrected Video sensor output, which was analyzed exclusively in all the tests, was routed through the high impedance loop of a Tektronix 1480R video waveform analyzer before being terminated in a Data Translation FG-100 frame grabber board. This board was installed in a PC. The FG-100 board provided the 75 ohm terminating impedance for the video signal chain. RG-59U coaxial cable (75 ohm impedance) was used exclusively to provide a balanced line. Existing frame analysis software was modified to account for the blank line characteristics of the IR Camera. The modified software permitted calculations of mean and standard deviation within a rectangular region whose size and location were user-selectable.

A Tektronix 2430 digital oscilloscope, fed from a "T" connector, was used to perform precision voltage and time difference measurements. Along with the frame analysis software, the 2430 was the primary measurement tool used in the tests. The 2430 was triggered off the "Line Sync" signal from the 1480R, which permitted any desired video line in the frame to be analyzed. A video monitor driven by the "Pix Monitor" output of the 1480R (an auxillary output that displays the video frame plus a line cursor), showed exactly which line in the frame was being measured by the 2430.

1.4 CALCULATION OF RADIOMETRIC QUANTITIES

In order to quantify irradiance levels at the telescope aperture, the procedure described below was used. For the tests involving radiometeric characterization, a adjustable-temperature blackbody source was used as the target. The blackbody is an Electro-Optics Industries (EOI) Model 1602V, which has a six-inch square active area and a temperature range of 50 - 600 degrees Celsius. The emitting surface of the source is painted with a high emissivity paint, and has a pattern of vertically oriented V-grooves (approximately 12 grooves per inch). The grooves increase the effective emissivity of the painted surface from 0.96 to 0.99 +/- 0.01 over the range 1 - 25 micormeters, according to the manufacturer. A precision resistance bridge is used in conjunction with platinum resistance temperature devices (RTDs) to monitor and control the source temperature to within +/- 0.5 degrees K. The source calibration provided by EOI was verified over a limited temperature range (up to about 120 deg. C) with an Everest Interscience Model 110 Radiometric Thermometer.

Because the spectral bandpass of the IR Camera encompasses several strong atmospheric absorption bands (e.g., the 4.3 um CO2 band), which affect even the relatively short laboratory path lengths, it was necessary to account for these bands in the calculation of source radiances. The LOWTRAN6 atmospheric model computer code was used for this purpose. It was operated in the radiance mode to compute the integrated radiance of the EOI source over the 200 inch (i.e., 5 meter) path length used in the lab. Radiances were calculated for each temperature employed and over each of the relevant

spectral sub-bands. The calculations were based on temperature and relative humidity measurements made during the sensor tests. The calculated spectral transmission of the path, along with the locations of the 3 spectral sub-bands, is shown in Figure 1-2. Note that all three bands are very near the edges of water vapor and/or carbon dioxide absorption bands.

The LOWTRAN-derived radiances were next corrected for the effects of the collimator, which has a reflectance of 0.97 +/- 0.01. Because its reflectance is wavelength-independent, the correction could be applied independently of the LOWTRAN calculations. The correction used was

$$\text{Corrected Radiance} = 0.97 * (\text{LOWTRAN Radiance}) + 0.03 * L(300\ K)$$

where L(300K) is the integrated radiance corresponding to the measured ambient temperature of 300 K (27 deg. C). This quantity multiplied by 0.03, the effective emissivity of the mirror, represents the self-emission of the collimator.

Finally, the collimator-corrected radiances were converted to irradiance per pixel at the telescope aperture by multiplying by the solid angle subtended by each detector element (8.E -10 steradians).

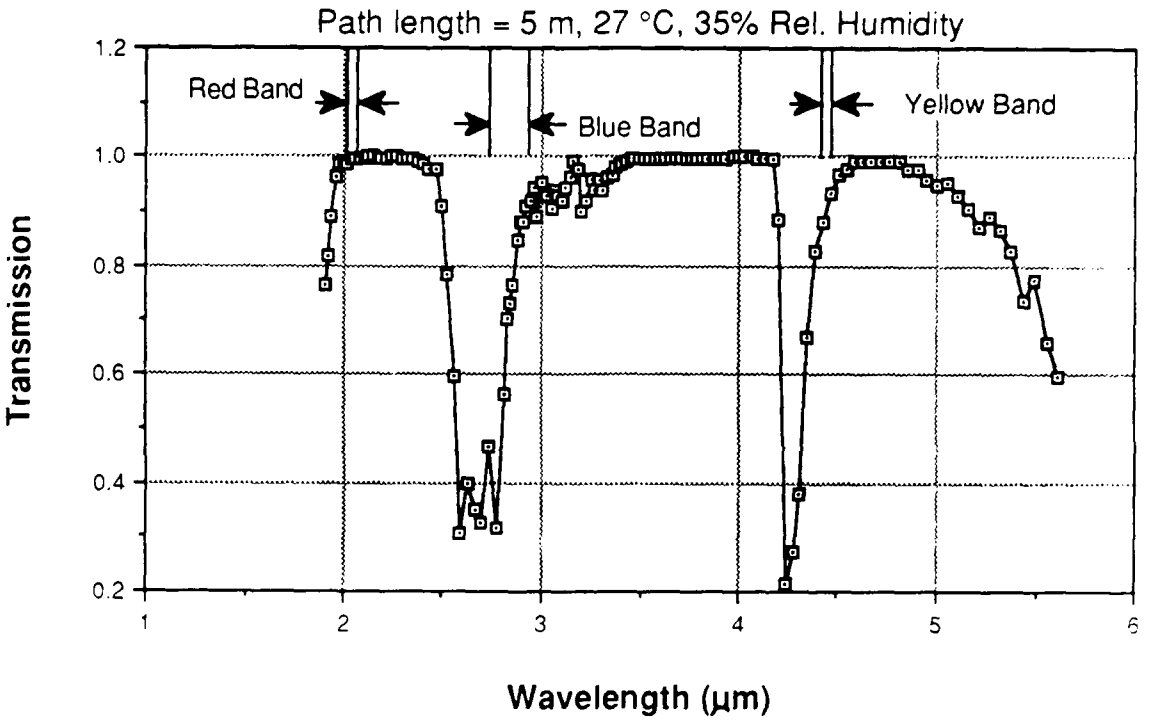

Figure 1-2. Atmospheric Spectral Transmission in Lab

2.0 CHARACTERIZATION TEST RESULTS

2.1 BLACK LEVEL RESPONSE TEST

2.1.1 Purpose

The Black Level control is a vernier calibrated ten-turn potentiometer that adjusts the bias voltage added to Corrected Video signal levels. The function of the bias is to ensure that no signals of interest are lost to black saturation; however, if too large a bias is used, very strong signal levels may be clipped at the high end of the output voltage range. In order to apply a single calibration relation to signals collected at an arbitrary Black Level setting, the corresponding bias level must be accounted for. The relationship between the amount of bias and the vernier readout must be characterized so that a suitable correction may be defined. The data collected to perform this task also provides information about the sensor output voltage range such as the maximum voltage level produced and the range of linear output.

2.1.2 Test Procedure

The IR Camera viewed the blackbody source with the latter unpowered so that its temperature was that of the ambient environment. The Reference Frame was stored while viewing the same blackbody so that a "zero-level" signal resulted; i.e., except for noise, each frame of data was equivalent to the Reference Frame, thus their difference was essentially zero. The black level control was set to its minimum value, 0.00, and the resulting average scene voltage was measured. This and all subsequent lab test voltage measurements were referenced to the "porch" of the horizontal sync pulse (i.e., zero IRE units in the RS-170 standard). It was verified that the porch level was independent of the Black Level control.

The voltage measurements were repeated for each of the four gain settings to assess whether there is any unexpected interaction between gain and offset. Because the scene equaled the Reference Frame, no signal variations with gain changes were expected. The Black Level control was increased in uniform increments up to its maximum setting of 10.00. Particular scrutiny was given to the range 0.50 to 1.50, as it is the range most often used during a data collection mission.

2.1.3 Test Results

The results over the full range of the Black Level control are shown in Figure 2-1 for gains of 8X and 1X. At the resolution of the plot, there is a small but distinct difference between the two. The test results for the 4X and 2X gain settings fall between the curves shown in Figure 2-1. Thus, a small dependence on gain level was observed. The voltage level versus Black Level setting characteristic

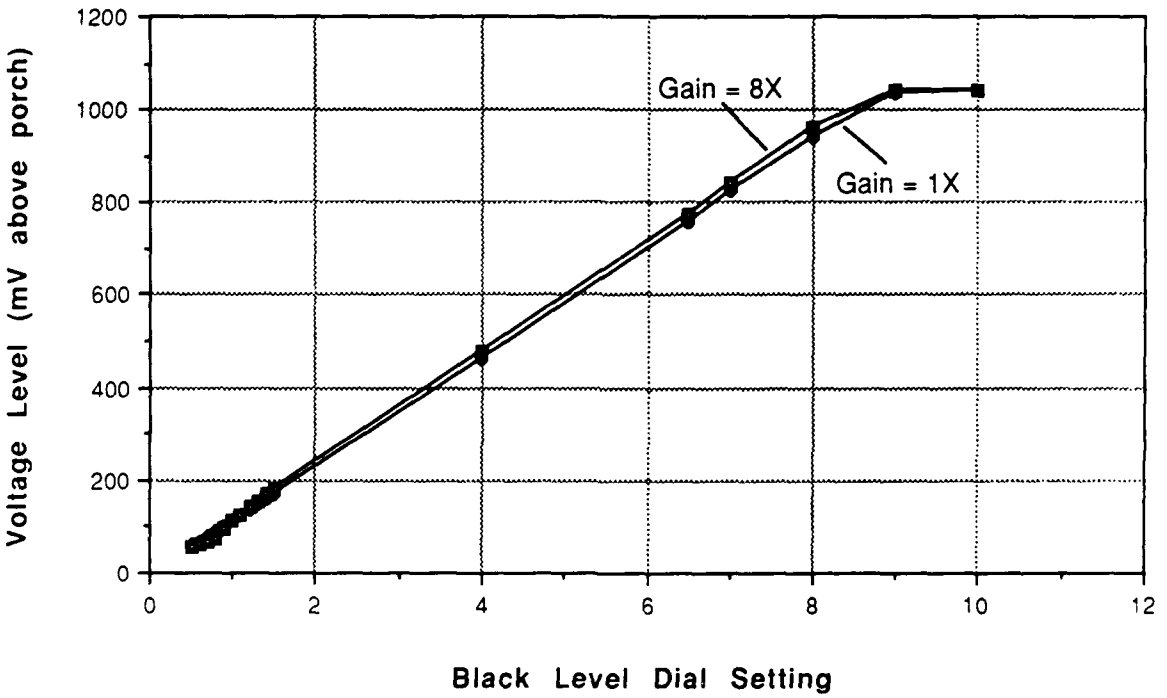

Figure 2-1. Ref. Frame Voltage vs. Black Level - Full Range

for any single gain setting is quite linear over the range 100 to 800 millivolts. Outside this range, slightly non-linear behavior is observed. Assuming the Black Level control itself is linear, these results indicate the linear region of the video output electronics.

Figures 2-2 and 2-3 show, for each gain level, the results of the Black Level test over the dial setting range of 0.50 to 1.50. At the top of each plot is the result of a linear regression analysis on the data. The points used in the regression were limited to dial range settings of 0.90 or greater. Below 0.90, non-linear behavior was observed; the degree of non-linearity appears to increase with gain level. Within the linear regions, the slopes of the curves also increase with the gain setting. The relative values of the slopes, referenced to the 1X value, are summarized in Table 2-1.

Table 2-1. Black Level Responsivities (mV/dial unit)

Gain:	1X	2X	4X	8X
Abs. Slope:	117.1	121.5	127.9	138.8
Rel. Slope:	1.000	1.038	1.093	1.185

The above results imply that a gain-specific Black Level correction is warranted when calibrating mission data. In addition, it appears that Black Level settings below 0.90 should be avoided, particularly at the higher gains, in order to avoid the non-linear regions shown in Figures 2-2 and 2-3.

The Black Level correction required for calibration of mission data should be only a simple offset correction based on the difference between the Black Level setting used in the mission and that used in the laboratory calibration test; i.e., it should take the form

$$\text{Corrected Voltage} = \text{Measured Voltage} + \text{Offset} \qquad (2\text{-}1)$$

where,

$$\text{Offset} = \text{Slope}(g) * [\ \text{BL(lab)} - \text{BL(mission)}\ ] \qquad (2\text{-}2a)$$

and

Slope(g) = Slope value from Table 2-1 for Gain "g"

BL(lab) = Black Level value used during lab calbration

BL(mission) = Black Level value used during mission.

Unfortunately, as will be seen in Section 2.2, a Black Level

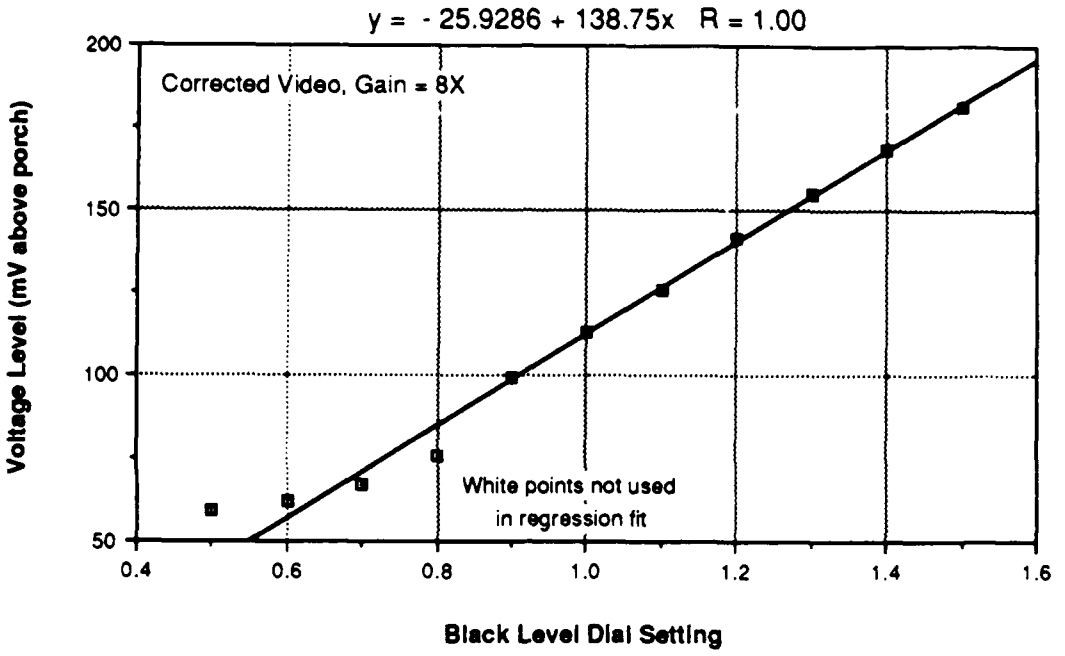

(a)

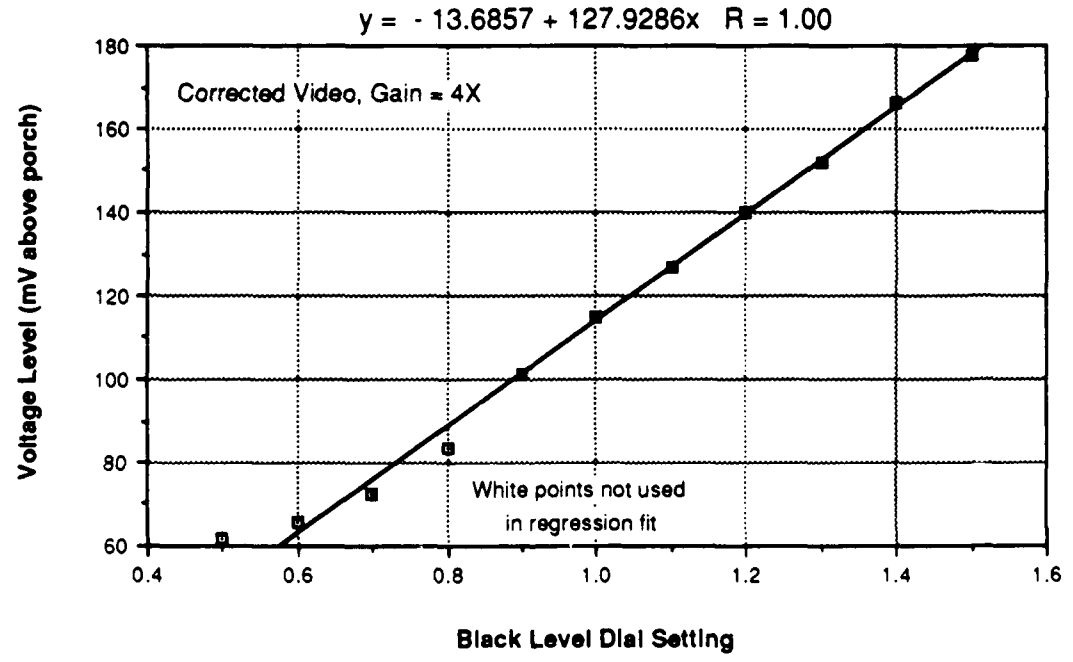

(b)

Figure 2-2. Reference Frame Voltage vs. Black Level

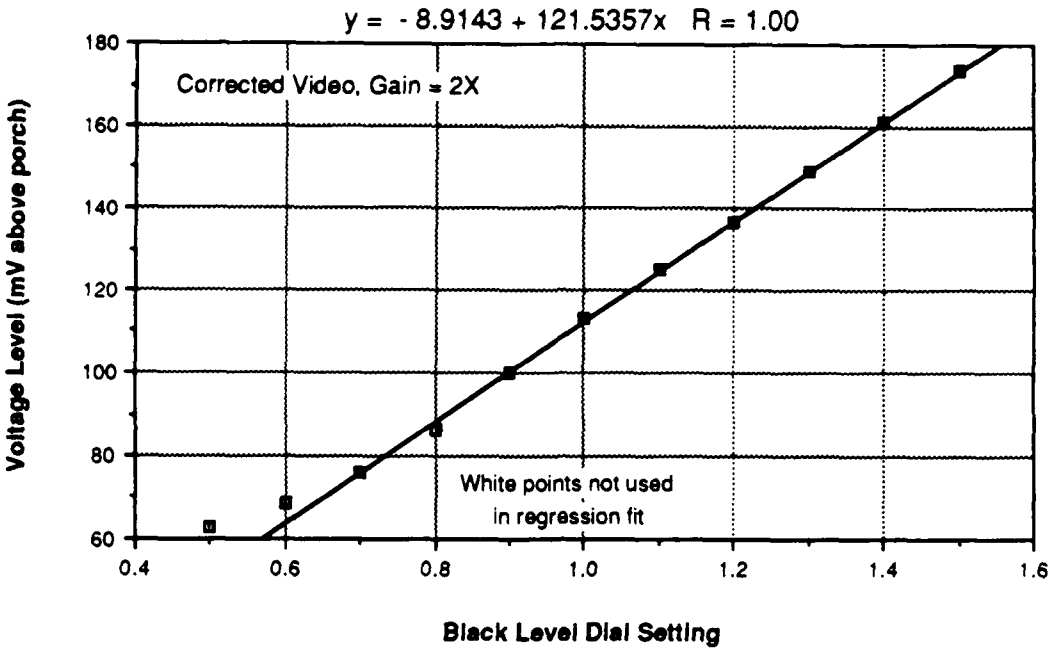

(a)

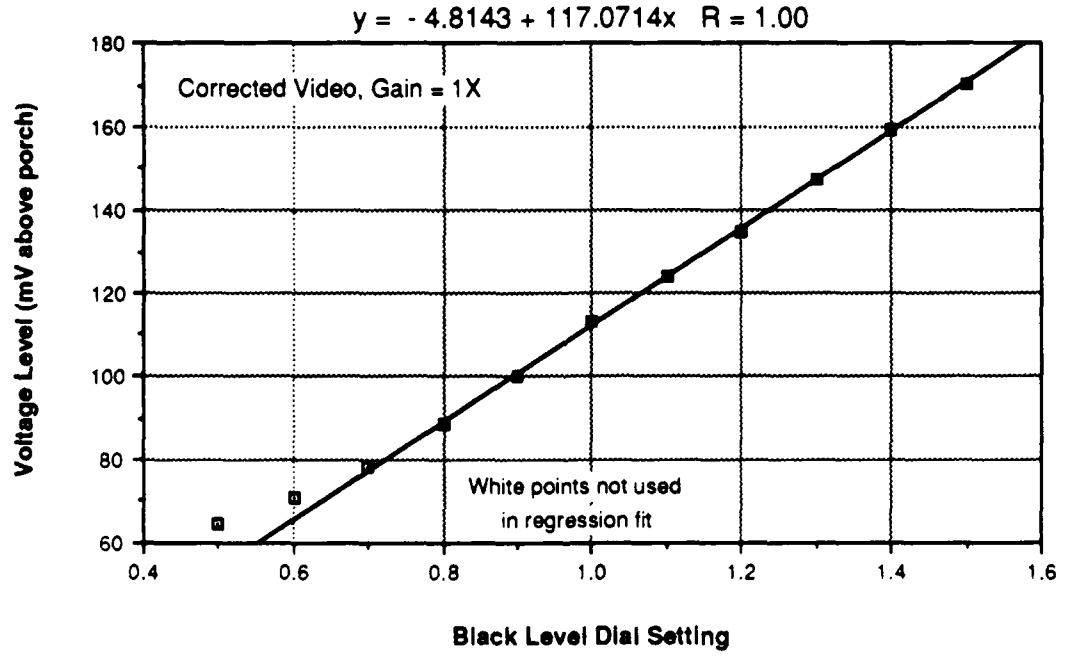

(b)

Figure 2-3. Reference Frame Voltage vs. Black Level

setting of 0.80 was used for the lab calibration of the broadband filter setting. (A setting of 1.20 was used in the calibration of the sub-bands.) The data points in Figures 2-2 and 2-3 deviate significantly at this setting from the linear relation defined for higher settings. Assuming these deviations represent a fixed, repeatable response, they may be accounted for by subtracting them from the Black Level offset correction defined by Equation 2-2a:

$$Offset = Slope(g) * [BL(lab)-BL(mission)] - Dev(g) \qquad (2\text{-}2b)$$

where "Dev(g)" is a gain-specific deviation term.

The final Black Level correction algorithm for broadband data is therefore defined by Equations 2-1 and 2-2b. The gain-specific values, Slope and Dev, required by Equation 2-2b are summarized in Table 2-2.

Table 2-2. Gain-Specific Values for Black Level Correction

Gain:	1X	2X	4X	8X
Slope:	117.1	121.5	127.9	138.8
Dev:	0.2	1.9	5.5	9.5

(Note: Slope units are [mV/dial unit]; Dev units are [mV])

A general Black Level correction procedure, applicable to any of the four filter settings, is given in Appendix B.

During the Black Level Response Test, the signal levels of the blank video lines (i.e., the lines not containing detector output) were also measured to determine what effect the Black Level control has over them. The results are shown in Figure 2-4 for both the full range of the Black Level control and the 0.50-1.50 range. As shown, the blank line signal increases linearly with Black Level setting, although the rate of increase is about ten percent of that observed in Figures 2-2 and 2-3. The rate is even lower in the 0.50-1.50 range; however, this is believed to reflect the non-linearity of the sensor output for signals below 100 millivolts.

The response characteristic of the FG-100 Frame Grabber was also determined from data collected during the Black Level Response Test. At each Black Level setting, the average digital level of the active lines was calculated. These values were then plotted against the voltage levels of the active lines to define the Digital Value vs. Video Signal Level characteristic shown in Figure 2-5. This characteristic was used in the analysis of the Broadband Signal Transfer Test data, as described in Section 2.2.2.

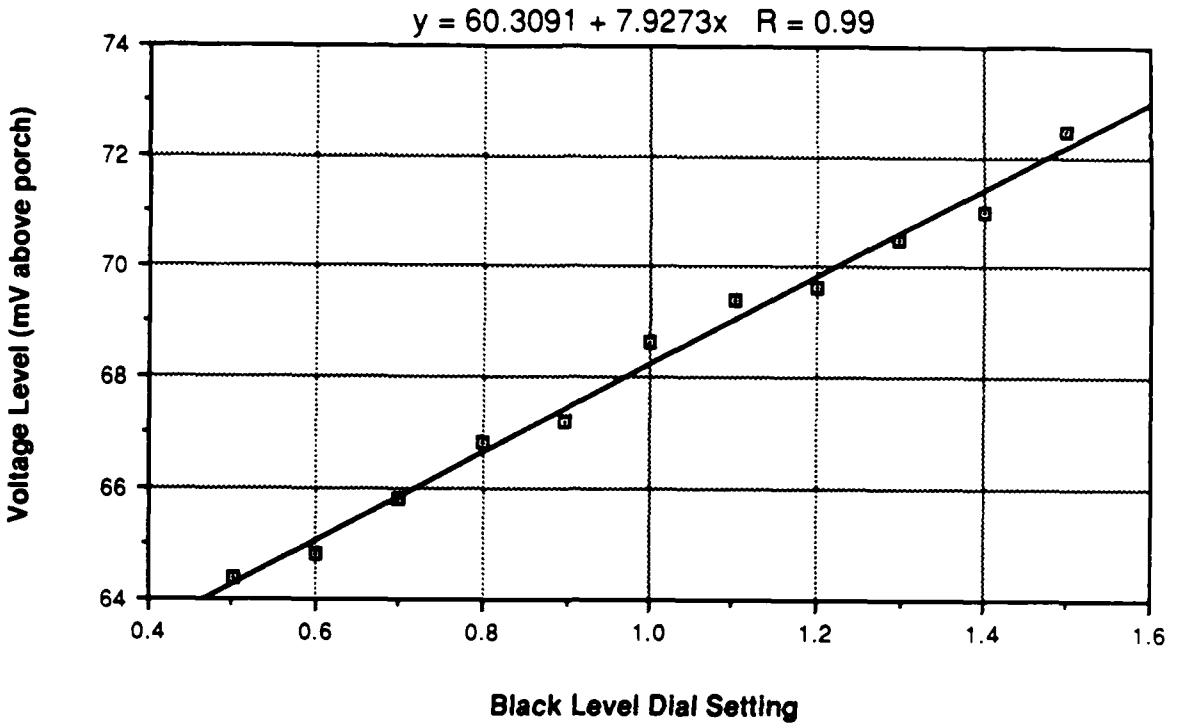

(a)

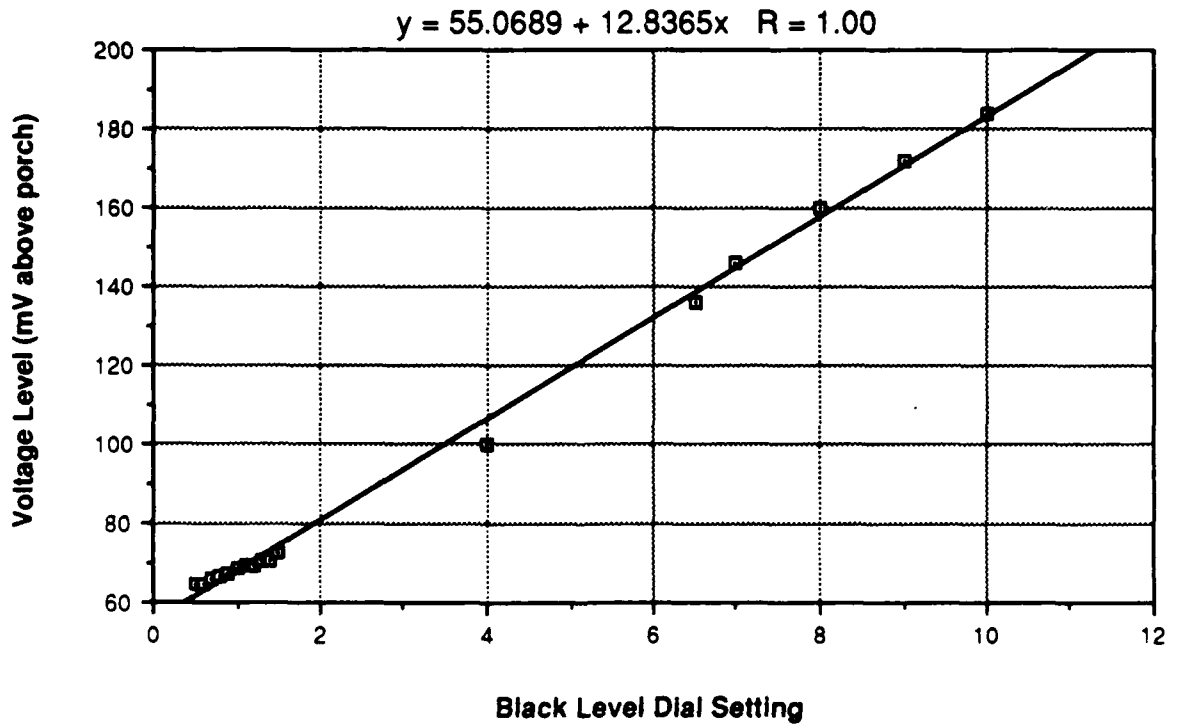

(b)

Figure 2-4. Blank Line Voltage vs. Black Level

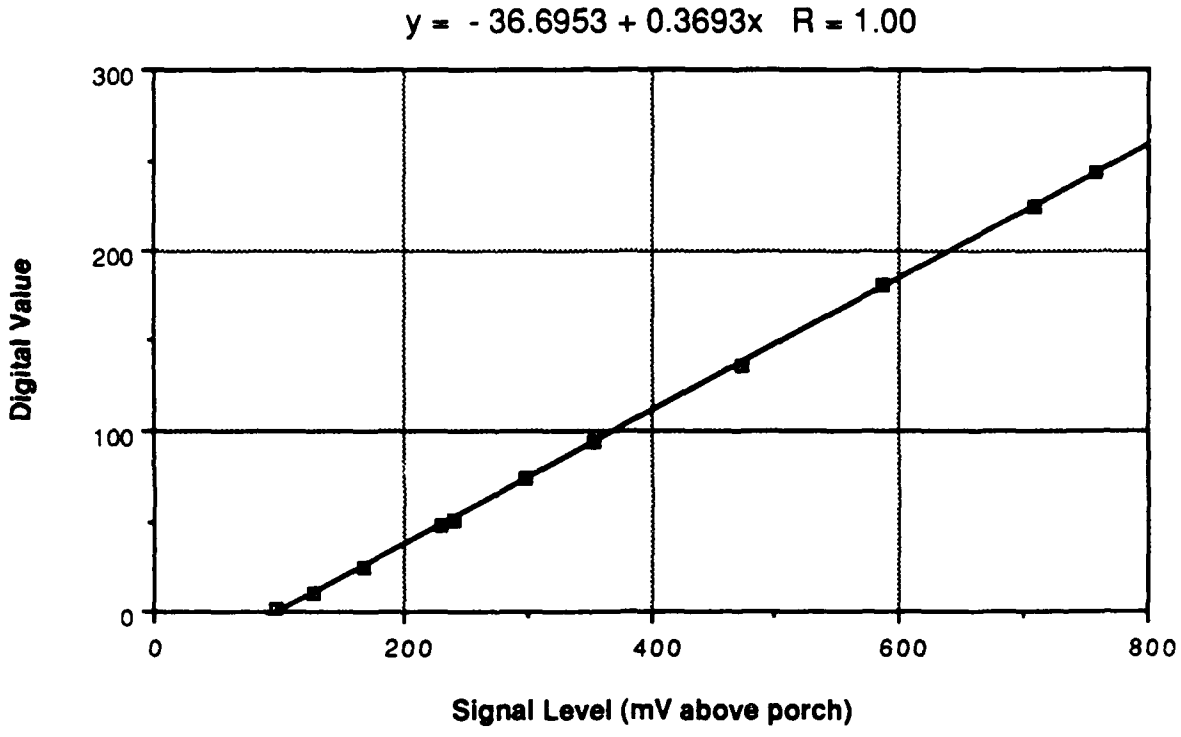

Figure 2-5. FG-100 Digital Value vs. Video Signal Level

2.2 BROADBAND SIGNAL TRANSFER TEST

2.2.1 Purpose

The purpose of this test was to define, for each of the four gain settings, a sensor calibration curve applicable to data collected with the open setting of the filter wheel, i.e., over the full spectral bandpass of the sensor. (Signal transfer tests were also conducted for each of the three sensor spectral sub-bands; these are described in Section 2.3.) The data collected during this test also define the upper limit of the system dynamic range for each gain, as well as provide responsivity data for defining radiometric sensitivity (cf., Section 2.4).

2.2.2 Test Procedure

The IR Camera was powered up and allowed to run for several hours in order to achieve internal temperature stabilization. A Reference Frame was stored by covering the telescope aperture with a piece of wood that had been cooled by pouring liquid nitrogen over it. The apparent temperature of the wood was approximately -40 deg. Celsius, as measured by the Everest radiometric thermometer. The EOI 1606V blackbody source was positioned at the collimator focal plane and heated to an initial temperature of 58 deg. C. The resulting sensor signal levels at each of the four gains were measured. The voltage level at the center of the field of view (FOV) was measured directly with the 2430 digital oscilloscope. The average voltage level over the entire FOV was determined indirectly by first measuring an average digital level with the FG-100 Frame Grabber, and then converting to voltage via the characteristic shown in Figure 2-5.

After making the set of signal measurements described above, the blackbody temperature was increased by approximately 20 degrees and allowed to stabilize. The signal levels corresponding to the new source temperature were then measured. This sequence was repeated until, for each gain, signals spanning the sensor dynamic range were observed. As the source temperatures increased, gain levels for which signal saturation was observed were no longer measured; i.e., measurements at 8X, 4X, and 2X gain were discontinued after the source temperature exceeded 111, 140, and 173 degrees Celsius, respectively. The source temperature was increased up to a maximum of 240 degrees, at which point saturation was observed with the 1X gain setting.

2.2.3 Test Results

The blackbody temperature values employed in the test were used to calculate irradiance levels at the telescope aperture via the procedure described in Section 1.4. The measured signal levels were plotted against these irradiances (in units of picowatts per square centimeter per detector) to define the signal transfer characteristic of each gain setting. The results for all four gains are summarized in Figure 2-6. The signal values shown represent the measured average over the entire field of view. The sensor parameters relevant to the

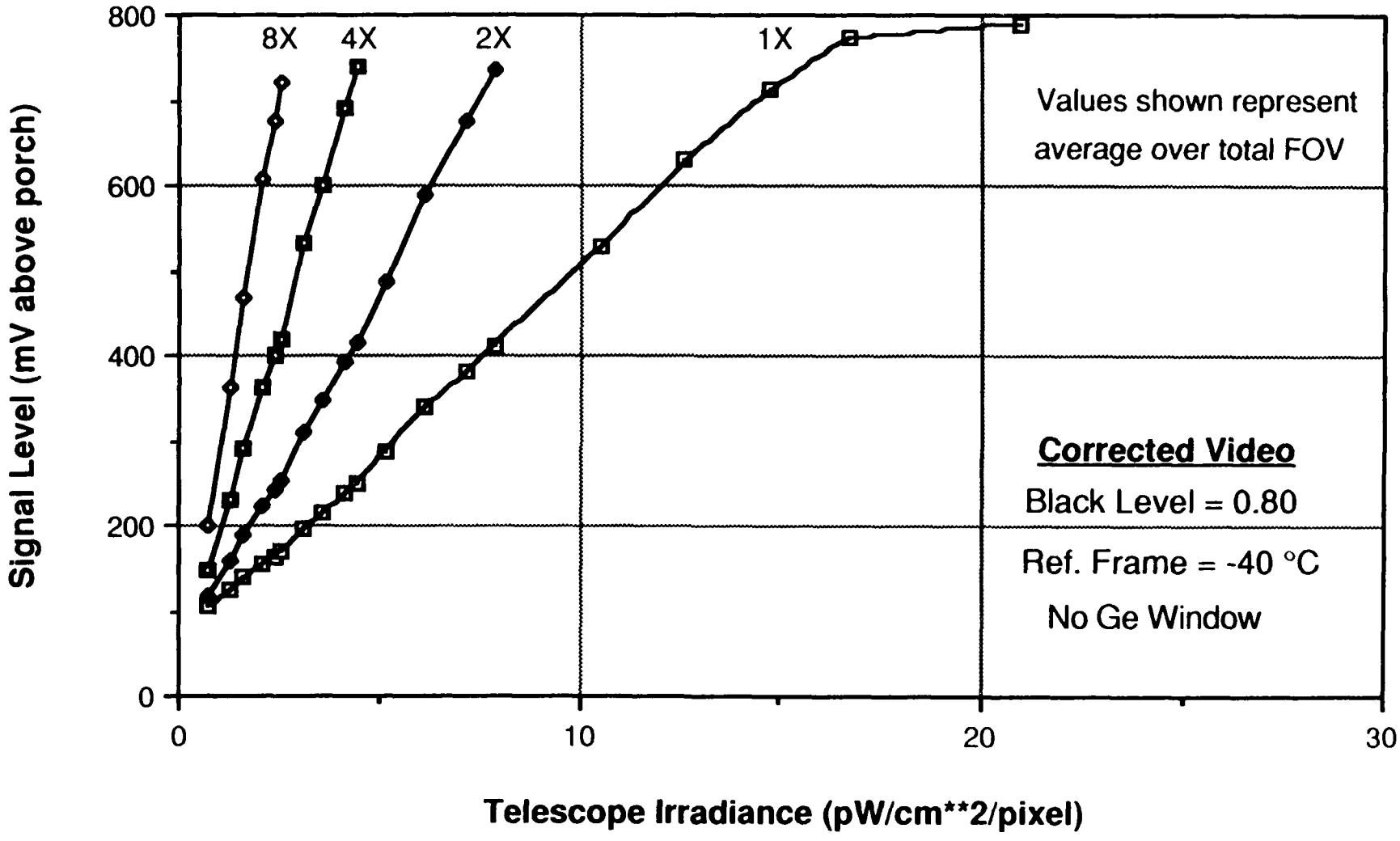

Figure 2-6. Summary of Broadband Signal Transfer Results

measurement results are shown in the figure. Data collected with different parameters, e.g., a different Black Level setting, must be corrected to the conditions of the lab test before the calibration values reported below may be used on them.

The test results for the individual gain levels are presented in Figures 2-7 through 2-10. A linear regression analysis was performed on the data collected for each gain, and results are shown at the top of each plot. The analysis for the 1X gain results, shown in Figure 2-7, omitted several points above 700 millivolts because non-linear behavior was observed. Recall that in the Black Level test, the linear range of the Corrected Video output extended to over 800 millivolts. Thus, the non-linear response shown in Figure 2-7 for input irradiances exceeding roughly 15 pW/cm**2 appears to represent saturation of the detectors themselves.

For irradiances below 15 pW/cm**2, the sensor exhibits essentially linear response. The deviations from linearity for each gain are plotted in Figure 2-11. Note that each gain is plotted with a different ordinate scale. The deviations, expressed in percent, were computed using the following formula:

$$\% \text{ deviation} = \frac{\text{measured signal} - \text{predicted signal}}{\text{predicted signal}} \times 100$$

where the "predicted signals" were obtained from the linear regression formulae shown in Figures 2-7 through 2-10.

As shown in Figure 2-11, significant percentage deviations from linearity were observed at gains of 1X and 2X for irradiances below 2 pW/cm**2. For the same irradiances at 4X and 8X gain (note that the first six points in each of the plots of Figure 2-11 represent the same irradiance levels.), the observed deviations are comparable to those observed at higher irradiance levels with all four gains. This suggests the deviations at the lower gains are the result of slight electronic non-linearities at signal levels below 200 millivolts (cf., Figures 2-7 and 2-8), even though such behavior was not indicated by the results of Section 2.1. For signal levels between 200 and 700 millivolts, the average absolute deviation from linearity for all the gain settings is one to two percent. This is comparable to the level of uncertainty associated with the blackbody source irradiances.

Figures 2-12 through 2-15 contain the signal transfer results for the voltages measured at the field of view (FOV) center with the 2430 oscilloscope. Linear regression results are again presented. Higher responsivity values (i.e., the slope term of the regression equation) were obtained for all four gains. To first order, this is believed to be due to vignetting effects, which reduce the average response over the FOV relative to the response at the center. For any video line whose signal levels were measured directly with 2430 scope, a decrease in response was observed that was symmetric about the FOV center. The

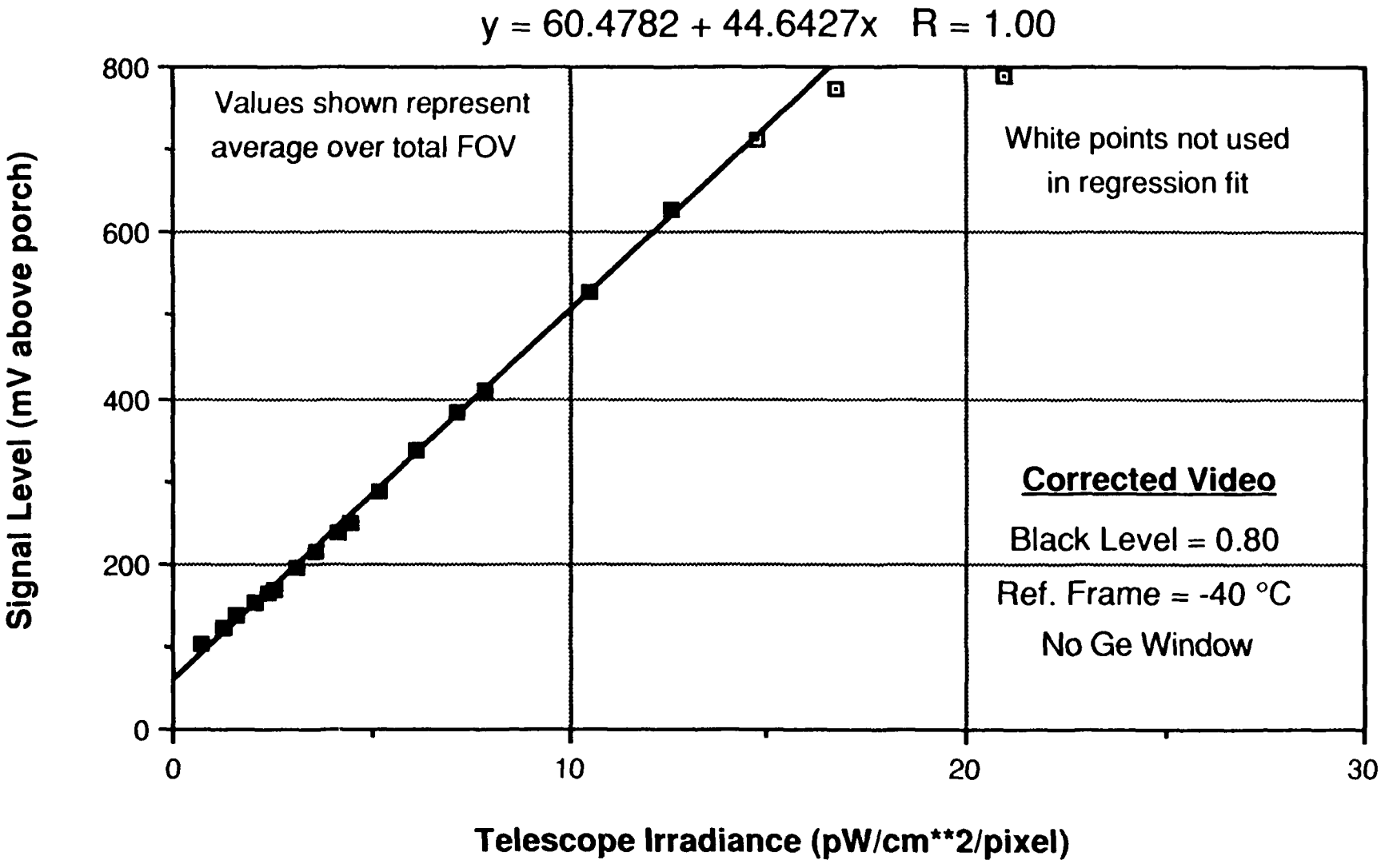

Figure 2-7. IR Imaging System Calibration - Gain = 1X

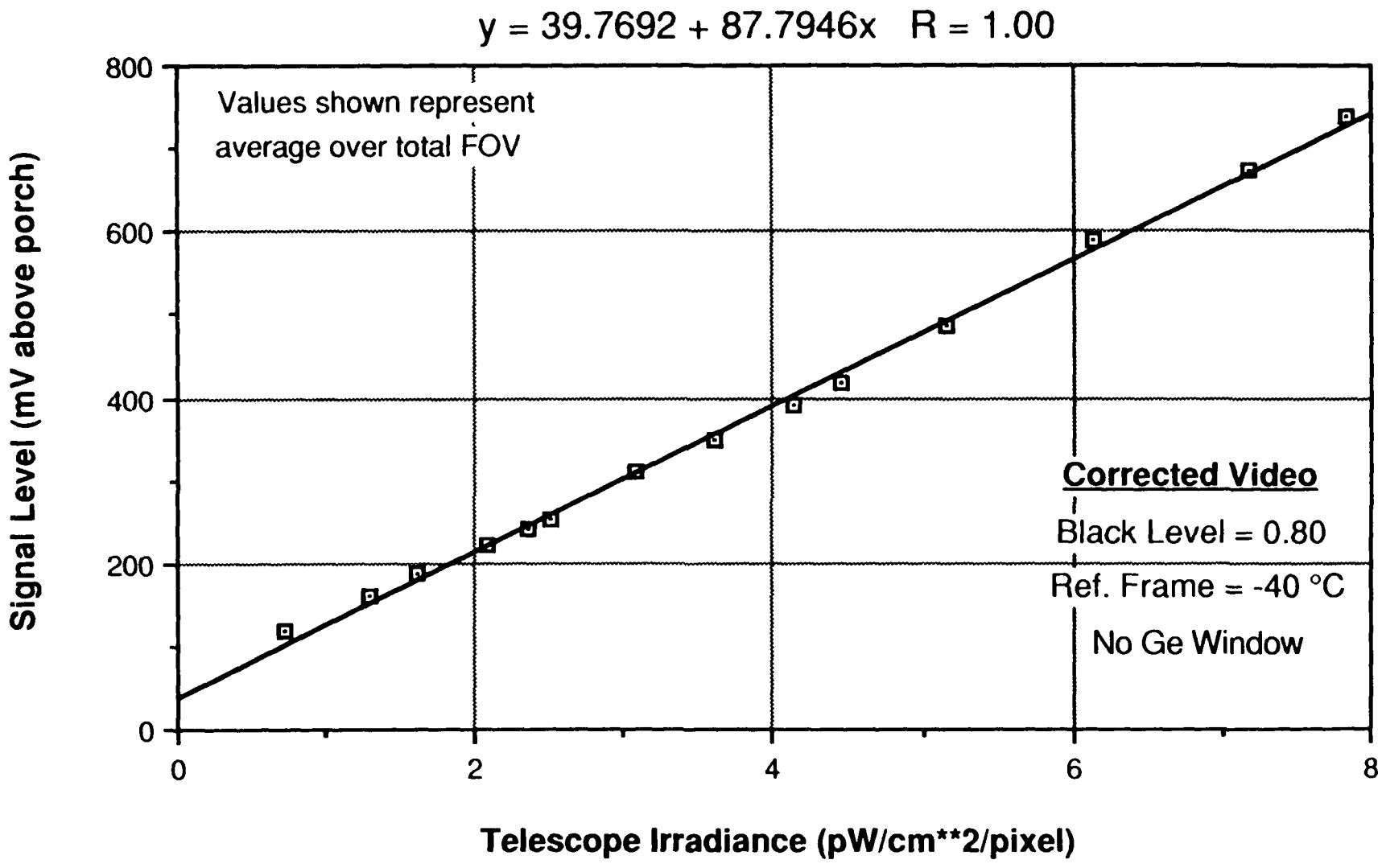

Figure 2-8. IR Imaging System Calibration - Gain = 2X

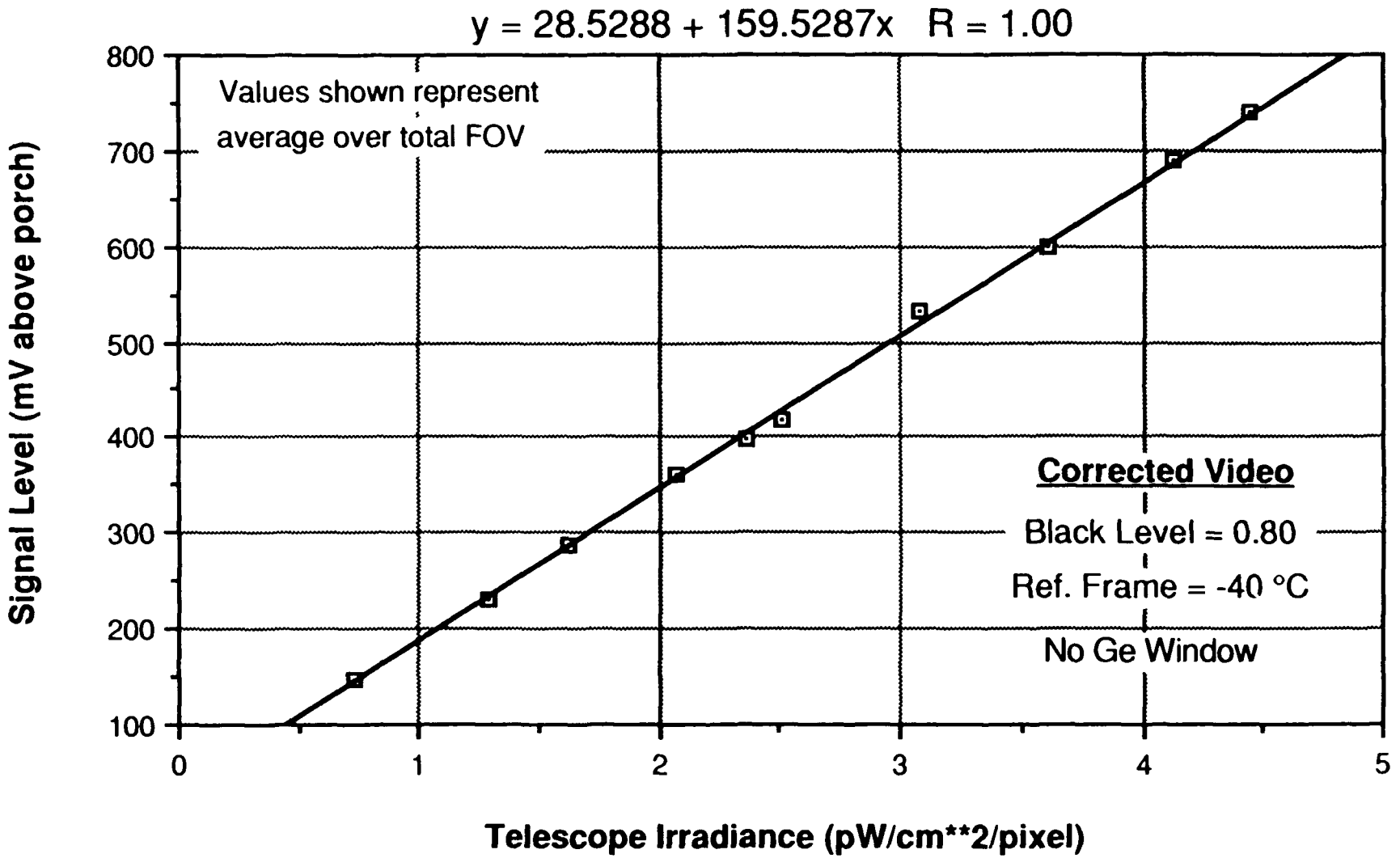

Figure 2-9. IR Imaging System Calibration - Gain = 4X

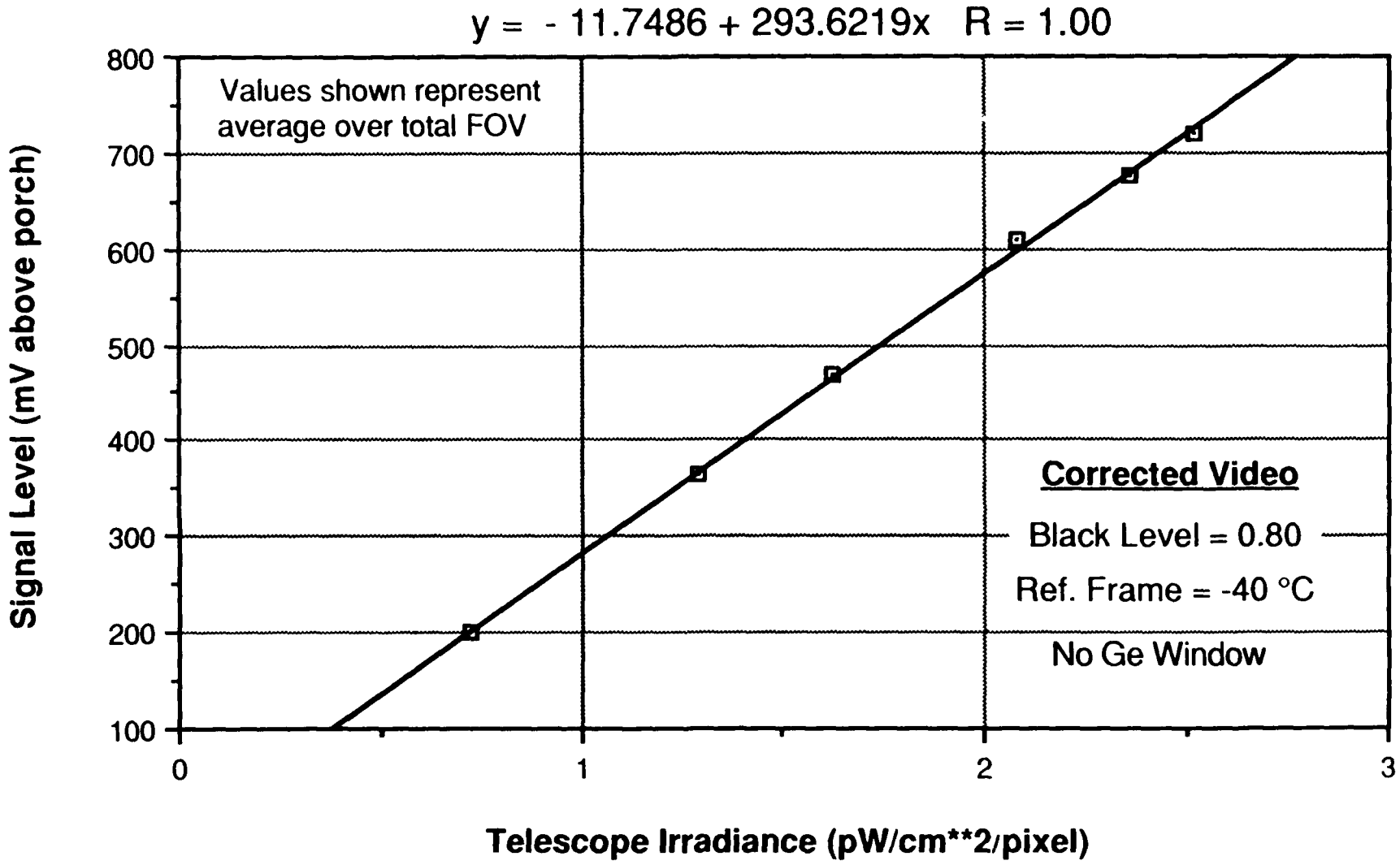

Figure 2-10. IR Imaging System Calibration - Gain = 8X

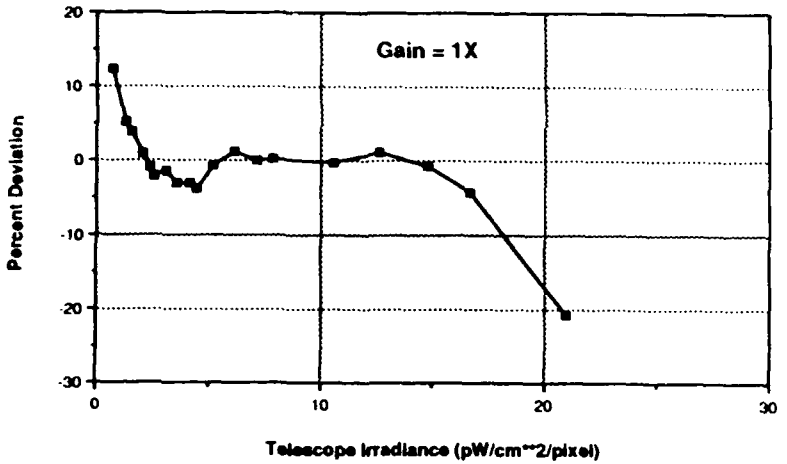

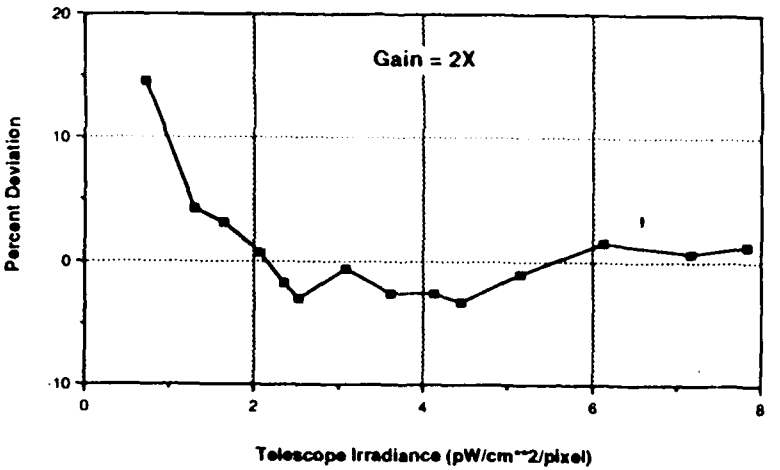

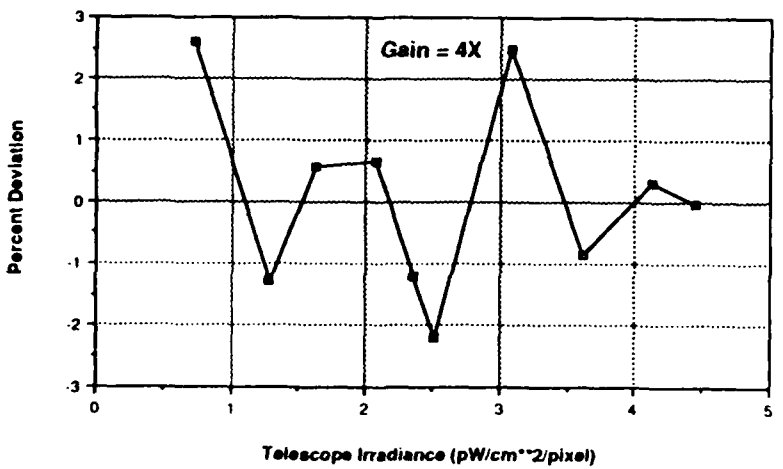

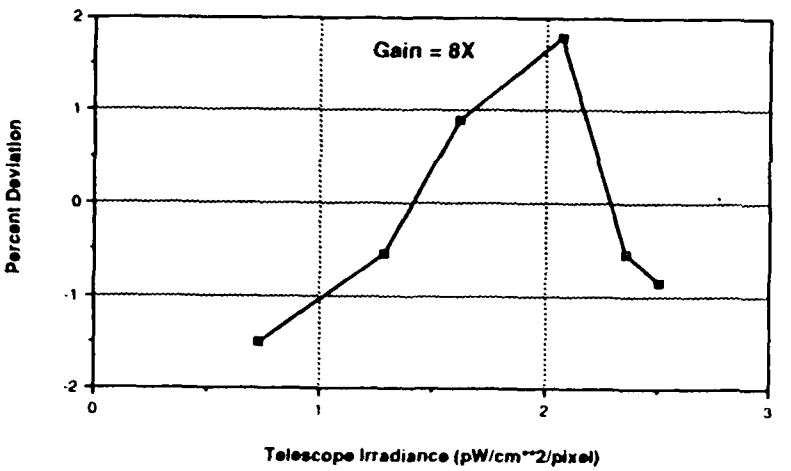

Figure 2-11. Deviation from Linearity vs. Irradiance

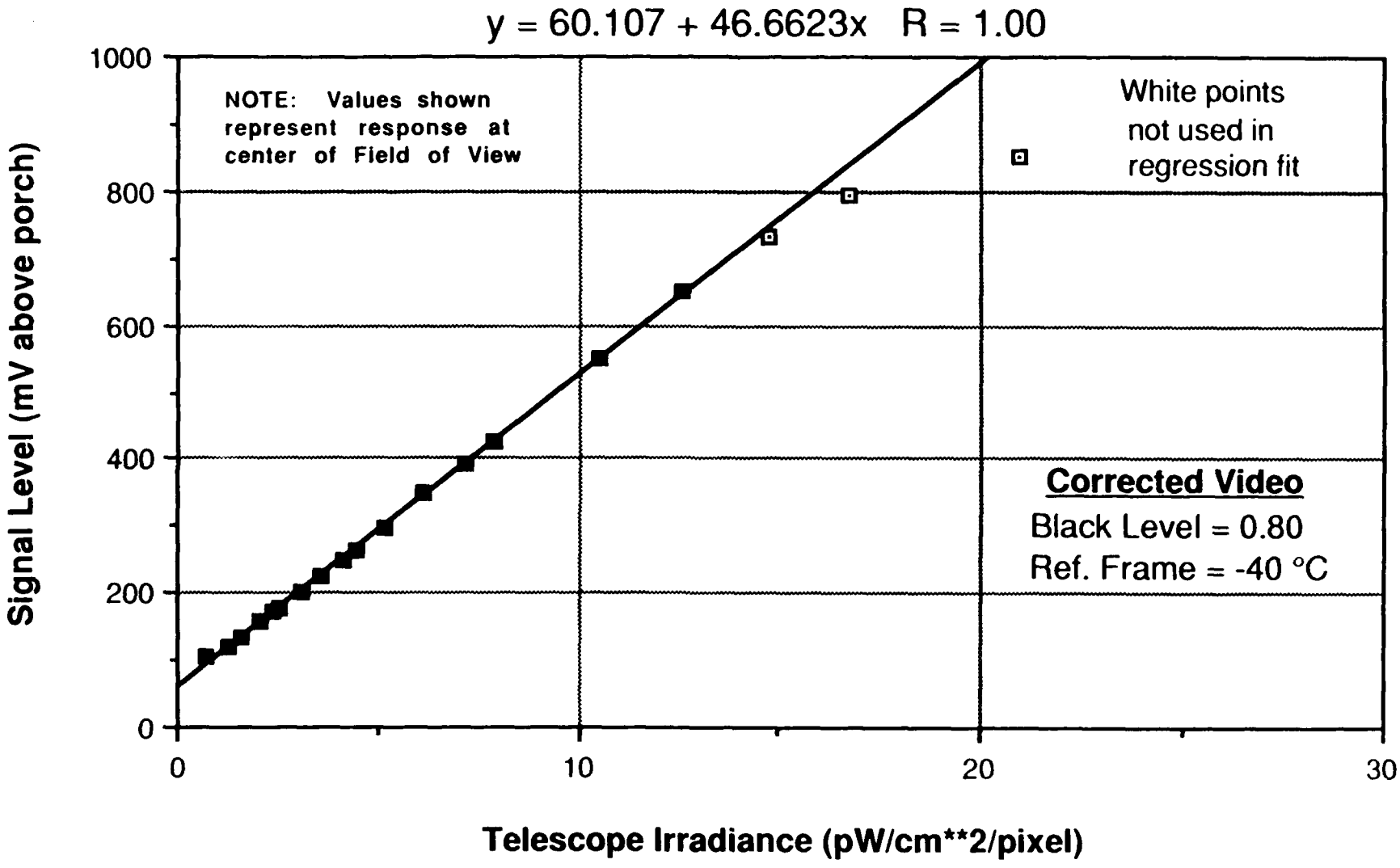

Figure 2-12. IR Imaging System Calibration - Gain = 1X

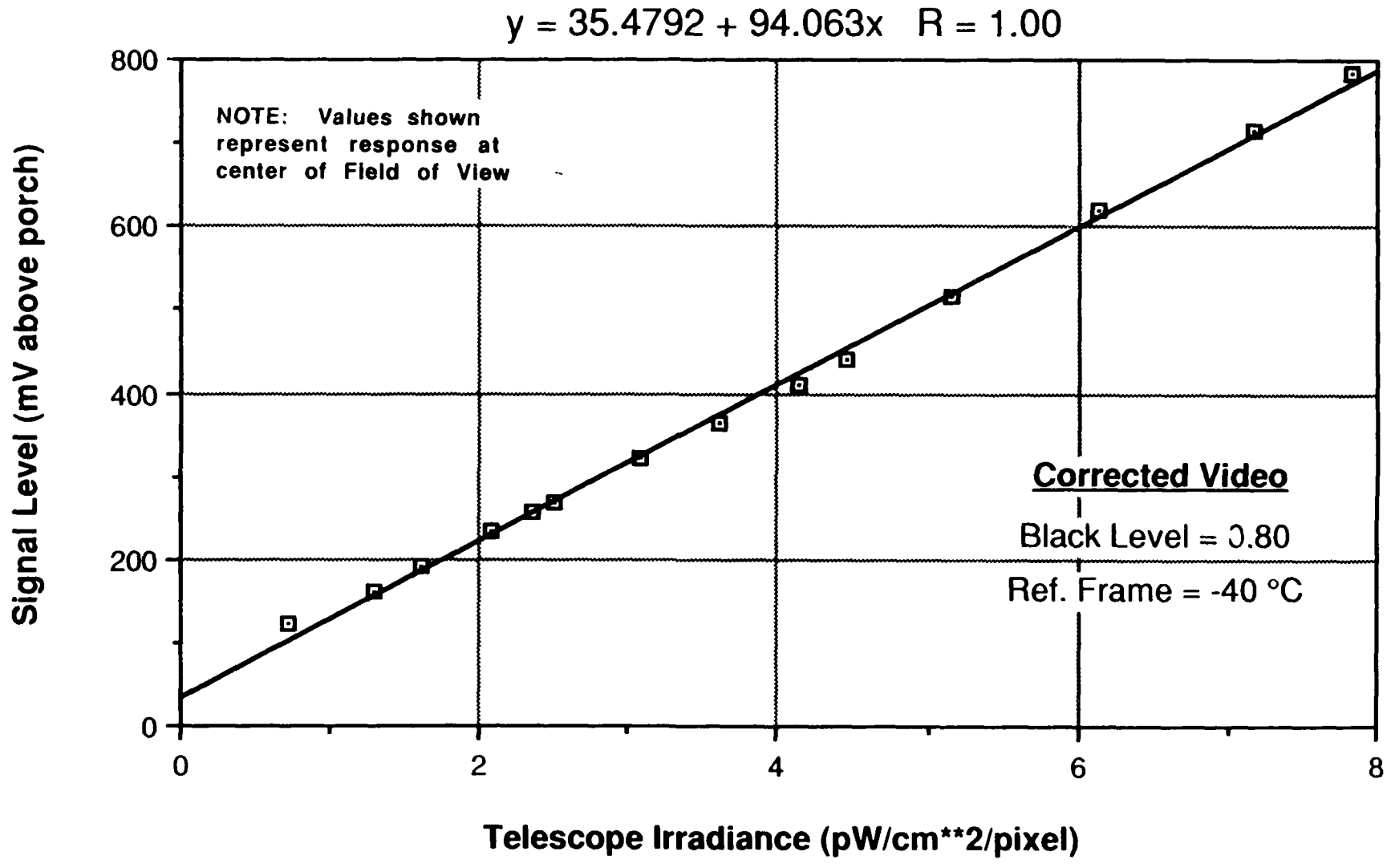

Figure 2-13. IR Imaging System Calibration - Gain = 2X

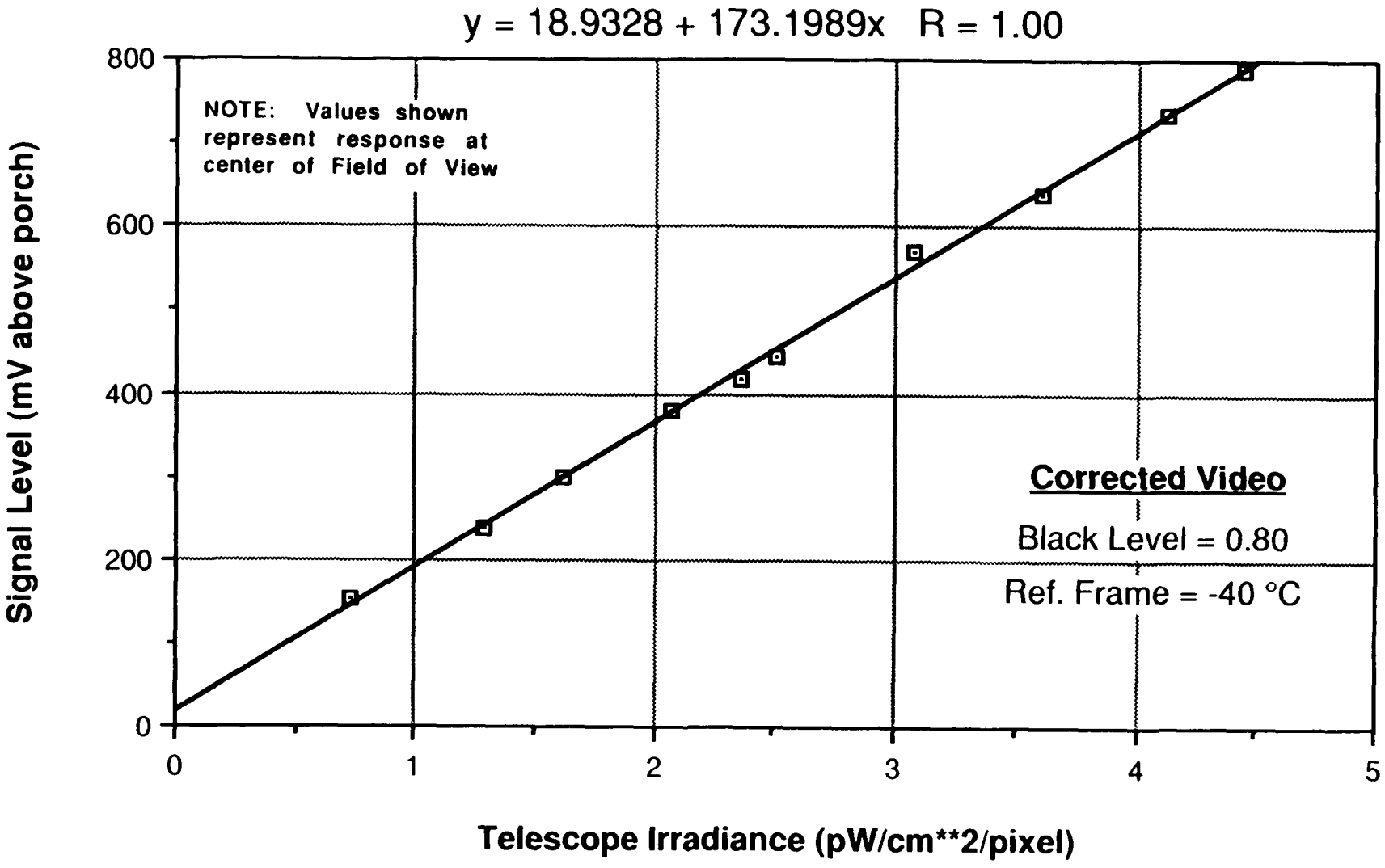

Figure 2-14. IR Imaging System Calibration - Gain = 4X

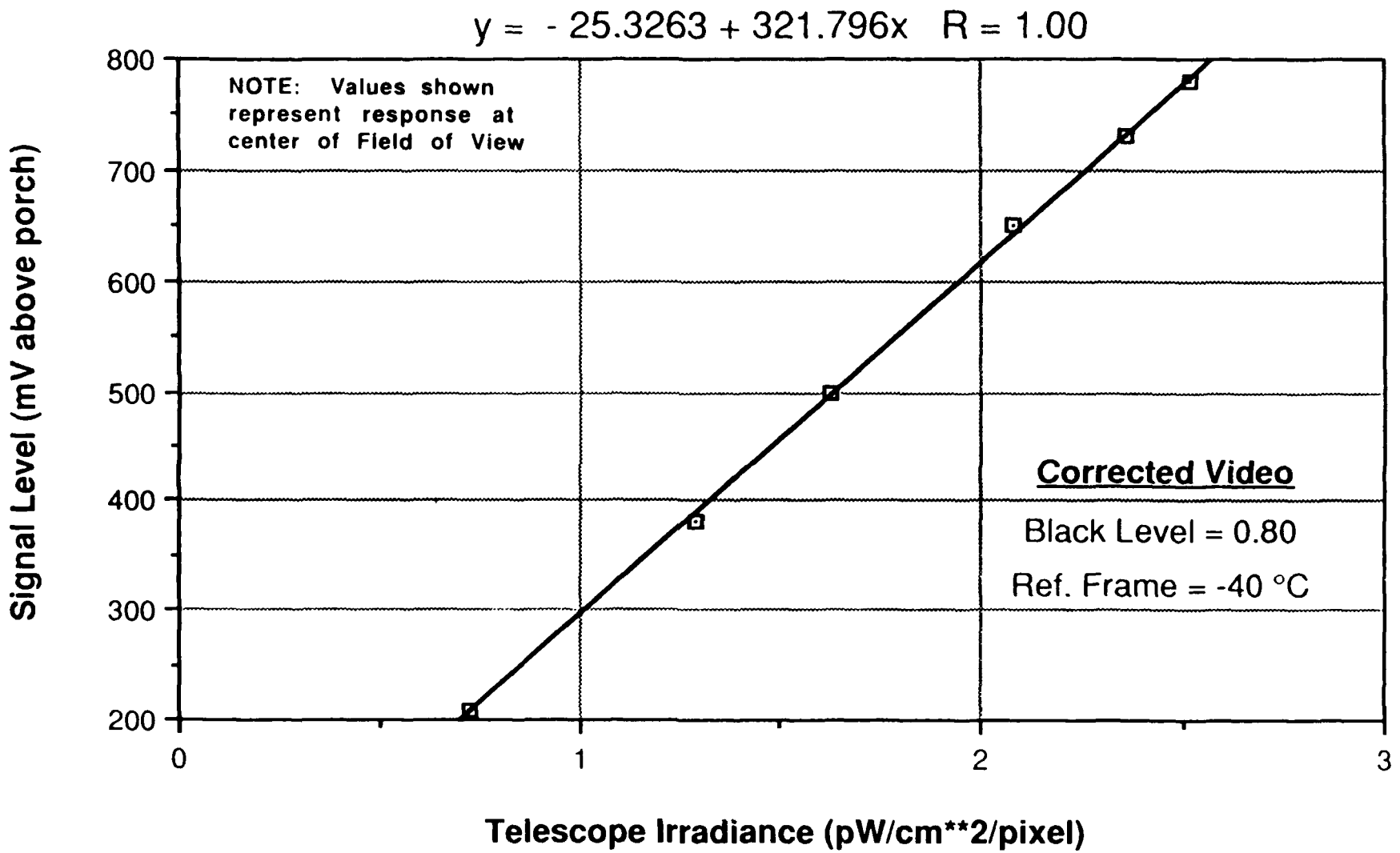

Figure 2-15. IR Imaging System Calibration - Gain = 8X

decrease in signal from center to edge was typically around ten percent. If this effect is purely optical, however, there should be no dependence upon gain level in terms of the response at the FOV center relative to that of the entire FOV. This was not observed in the data. The table below summarizes the responsivities at the FOV center and over the entire FOV, as well as their ratio, for each gain.

Table 2-3. Measured Broadband Responsivities [mV/(pW/cm**2)]

Gain	FOV Center	Entire FOV	Ratio
1X	46.66	44.64	1.045
2X	94.06	87.79	1.071
4X	173.20	159.53	1.086
8X	321.80	293.62	1.096

Table 2-3 shows a small but consistent increase with gain level in the ratio of the two responsivities. The ratio values should be the same for each gain level if optical vignetting were the only effect present. The fact that they are not suggests that some electronic phenomenon is also involved. The exact nature of the phenomenon is not understood; however, the effect is small enough to ignore as long as each gain setting is treated independently.

The responsivity values of Table 2-3 may be used to quantify the actual gain levels, relative to the value at 1X, of the three higher gain settings. The results are shown in Table 2-4. At the 4X and 8X settings, the relative gains are ten to fifteen percent below their nominal values.

Table 2-4. Relative Gain Levels from Broadband Responsivities

Gain:	1X	2X	4X	8X
Entire FOV:	1.	2.0	3.6	6.6
Center FOV:	1.	2.0	3.7	6.9

The linear regression results of Figures 2-7 through 2-10 represent the sensor calibration obtained from the lab tests. The procedure for calibrating mission data based on these results is summarized in Appendix B.

2.3 SPECTRAL SUB-BANDS SIGNAL TRANSFER TEST

2.3.1 Purpose

The purpose of this test was to characterize the response of the IR Camera's three spectral sub-bands in order to: (1) define a radiometric calibration relation for each sub-band; (2) provide responsivity data that would permit calculation of NESR within each sub-band (cf., Section 2.4); and (3) assess the relative spectral response of the PtSi FPA. Table 2-5 summarizes the characteristics of the bandpass filters associated with the three sub-bands.

Table 2-5. Summary of Bandpass Filter Characteristics

Color Designation	Center Wavelength	Half-power Bandwidth	Peak Transmittance
RED	2.040 um	0.090 um	0.78
BLUE	2.804 um	0.254 um	0.79
YELLOW	4.484 um	0.075 um	0.75

2.3.2 Test Procedure

The procedure employed for this test was nearly identical to that described in Section 2.2.2 for the Broadband Signal Transfer Test. The only differences were: (1) the 8X gain setting was used exclusively; (2) different blackbody source temperatures were used; and (3) only signal levels at the FOV center were measured; and (4) a Reference Frame was stored before each signal measurement in each sub-band.

The requirement for storage of a Reference Frame before each signal measurement arose from two factors. The first was the observation that a single Reference Frame--which, of necessity, must be collected at one of the four possible filter wheel settings--is not appropriate for data collection at all four filter wheel settings. The reasons for this are discussed in detail in Section 2.5.1. For now, it is sufficient to state that the Reference Frame collected at one filter setting represents an offset signal that may be too large or too small for any other setting.

The second reason for storing a Reference Frame before each voltage measurement was the desire to collect data in all three sub-bands simultaneously for each blackbody temperature used. This shortened and simplified the data collection process, since the blackbody only had to be heated through the sequence of temperatures one time. This approach required that a repeatable Reference Frame

temperature was available. The same wooden plate used for the Broadband Signal Transfer Test was used for this purpose. Its temperature was kept constant by keeping it in a freezer between data measurements. Its effective radiometric temperature using this procedure was roughly -5 to -7 degrees Celsius. Prior to the test, it was determined that the sensor response was virtually unchanged by a Reference Frame at -5 degrees C compared to one at -40 degrees.

2.3.3 Test Results

Using the procedure described in Section 1.4, the blackbody temperatures used in the test were converted into in-band radiances for each sub-band, and then divided by the respective half-power bandwidths (Table 2-5) to define effective spectral radiances. Plots of the measured signal levels for each sub-band versus these spectral radiances appear in Figures 2-16, 2-17, and 2-18. Note that while highly linear responses were observed in the Blue and Yellow sub-bands, the Red sub-band response steadily decreased with increasing radiance. A third-order polynomial was found to fit the observed response quite well, and is shown in Figure 2-16. There is no obvious explanation for the observed lack of linear response in the Red sub-band.

An analysis of the observed sub-band responses was made in order to assess the relative spectral response of the sensor. Measured responsivities from only three narrow spectral bands do not, by themselves, permit a very detailed spectral response characterization. For PtSi detectors, however, an analytic form for R_det(λ) the detector response at wavelength λ, is widely used, viz.,

$$R\_det(\lambda) = C1 \left(1 - \lambda / \lambda_c \right)^{**2} \qquad (2\text{-}3)$$

where C1 is a constant having units of amps per watt, and λ_c is the detector cut-off wavelength, which is determined by the Schottky barrier potential of the device. If the assumption is made that the various optical elements of the sensor, excluding the spectral filters, have transmittances that are essentially wavelength-independent over the detector's responsive range, then the relative spectral response of the entire sensor should follow the functional form of Equation 2-3. This assumption can be tested using the measured sub-band responsivities.

Consider a ratio of R_det values at two different wavelengths λ_1 and λ_2. Denoting this ratio as K, it is easily shown to have the form:

$$\frac{R\_det(\lambda_1)}{R\_det(\lambda_2)} = K = \left[\frac{\lambda_c - \lambda_1}{\lambda_c - \lambda_2} \right]^{**2} \qquad (2\text{-}4)$$

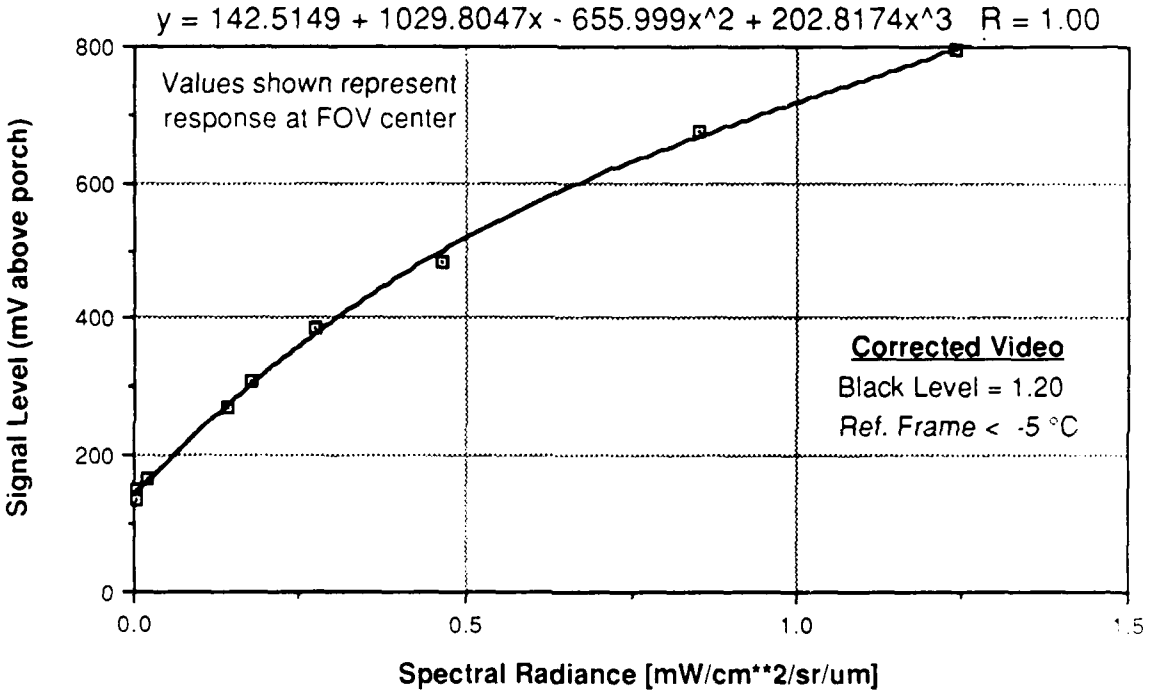

(Note: Inverse of polynomial regression result is

x = -0.123 + 8.453e-4y + 1.009e-8y^2 + 1.345e-9y^3)

Figure 2-16. Signal Transfer Results - Red Band (2.04 um)

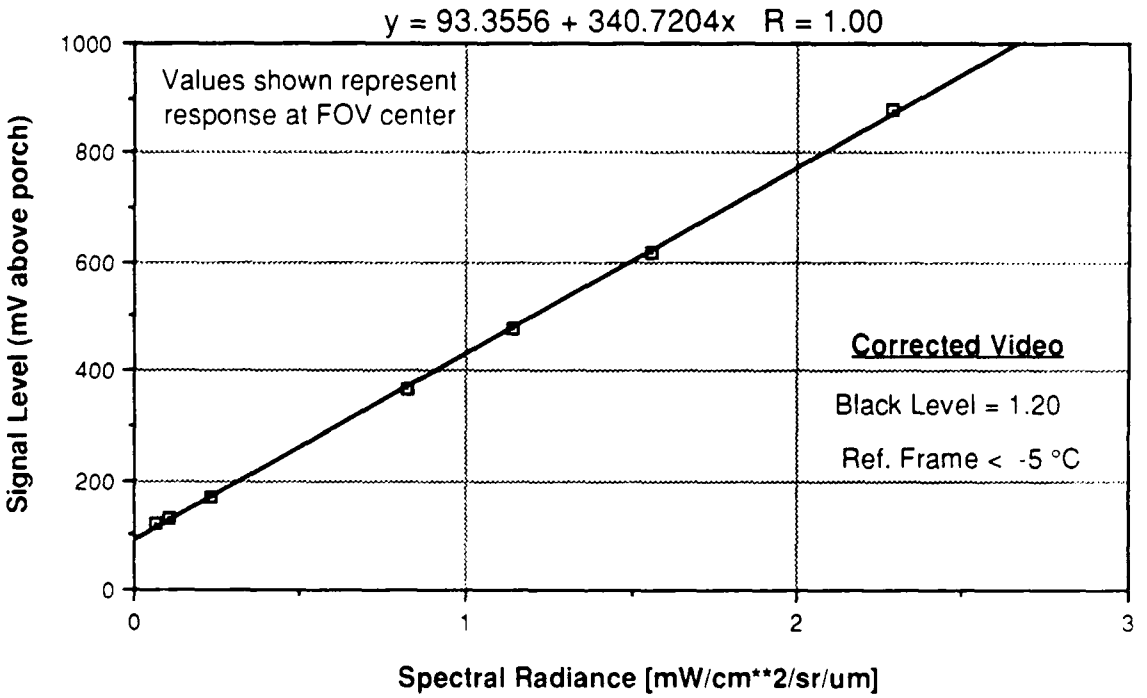

Figure 2-17. Signal Transfer Results - Blue Band (2.805 μm)

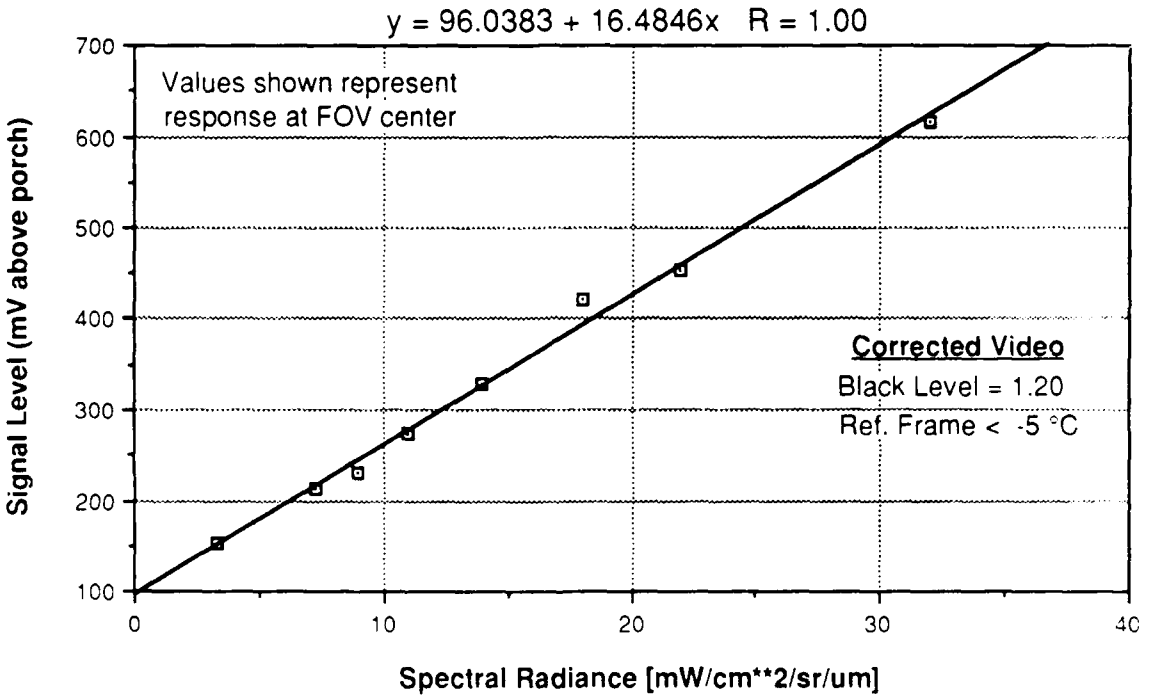

Figure 2-18. Signal Transfer Results - Yellow Band (4.484 μm)

Equation 2-4 defines the relationship between cut-off wavelength λ_c and spectral response ratio K. Given the former, the latter may be computed for any two wavelengths. In the original IR Camera Calibration Report produced by David Sarnoff Research Center, the Schottky barrier potential of the detector array is listed as 0.221 eV, which corresponds to a cut-off wavelength λ_c of 5.61 um. This value may be used in Equation 2-4 to predict values of K using the center wavelengths of the three spectral sub-bands. The measured sub-band responsivities may then be ratioed and compared to the predicted values. The level of agreement between the two sets of ratio values indicates how well the sensor spectral response matches the form of Equation 2-3.

The analysis procedure described above was performed and yielded the results shown in Tables 2-6 and 2-7. Table 2-6 summarizes the responsivity values used to compute spectral response ratios. The column labeled "Measured Responsivity" corresponds to the slope values from Figures 2-16 through 2-18. Note that for the RED band (Figure 2-16), responsivity is a function of scene radiance. The value obtained at an arbitrarily chosen level of 1.0 mW/(cm**2 sr um) was used in the analysis. The column in Table 2-6 labeled "Corrected Responsivity" contains values that have been adjusted to remove the effects of the spectral filters, specifically, bandwidth and peak transmission.

The comparison between measured and calculated spectral response ratio is shown in Table 2-7. Note that the measured ratios involving the Red band are significantly higher than predicted by Equation 2-4, while the Blue/Yellow ratio agreement is reasonably good. The small amount of data precludes any definitive explanations; however, one interpretation of the Table 2-7 results is that the sensor spectral response follows Equation 2-4 fairly well, but the Red sub-band response is somewhat higher than expected, the Blue response is slightly lower than expected and/or the Yellow response is slightly greater than expected. Subtle changes in the spectral filter cnaracteristics since the time of their measurement could explain these deviations.

2.4 NOISE/SENSITIVITY CHARACTERIZATION

2.4.1 Purpose

The radiometric sensitivity of the IR Camera may be defined as the ratio of RMS noise level to responsivity, i.e.,

$$\text{Noise Equivalent (unit)} = \frac{\text{rms noise in millivolts}}{\text{responsivity in mV/(unit)}} \qquad (2\text{-}5)$$

where "unit" is whatever radiometric quantity is of interest, e.g., irradiance, radiance, spectral radiance, etc.

Table 2-6. Sub-Band Responsivity

Sub-Band Designation	Center Wavelength	Measured* Responsivity	Corrected** Responsivity
RED	2.04 μm	326.†	3620.
BLUE	2.085 μm	341.	1340
YELLOW	4.484 μm	16.5	220.

(* units are mV per mW/cm**2 sr μm)

(** units are mV per mW/cm**2 sr)

(† value @ 1.0 mW/cm**2 sr μm, cf. Figure 2-16)

Table 2-7. Spectral Response Ratios

Ratio	K(measured)*	K(calculated)**	Difference
RED/BLUE	2.60	1.62	+ 60 %
RED/YELLOW	13.7	10.1	+ 36 %
BLUE/YELLOW	5.79	6.21	- 7 %

(* from Table 2-6 data)

(** from Equation 2-4 @ cut-off wavelength = 5.61 μm)

Responsivity values have already been reported in Sections 2.2 and 2.3 for the various gain levels and spectral sub-bands. A specification of noise level is therefore all that is required in order to use Equation 2-5. For a single-element detector, this would be a simple task; however, for a focal plane array, the definition of noise level, i.e., the limit of measurement precision, is not as straightforward. For a point source target, whose signal represents a single detector element's output, the quantity of interest is the temporal noise associated with that element. This is the equivalent of the single-element detector case, and is typically the criterion used to specify the "Noise Equivalent" performance level of the FPA. For extended targets such as plumes, however, signals from many individual elements are available for measurement. The precision with which signal differences between separate elements may be measured is limited not only by temporal noise, but also by uncertainties associated with the unique response characteristics of each element. This latter factor is usually referred to as "fixed-pattern noise," or simply, "pattern noise." It is not a noise in the stochastic sense, but does contribute to the rms deviation observed in any region of pixels.

In principle, pattern effects are deterministic, and therefore may be characterized and removed. For example, if each detector element is modeled as being a linear system, a gain and offset may be measured for each, and a pixel-by-pixel correction algorithm defined. Such a scheme requires at least two known points from each detector's response curve, and thus, is referred to as a two-point correction. In the IR Camera, the Reference Frame subtraction used with the Corrected Video output performs a one-point correction. This approach can only provide an offset correction (which will never be perfect) over the FPA. Responsivity differences between detector elements remain to introduce pattern noise, the magnitude of which is linearly proportional to the target signal being received (or, more precisely, to the difference between the target energy and the energy of whatever scene was viewed when the Reference Frame was stored).

Based on the above considerations, the objective of the noise characterization tests was to define the relative contributions of temporal noise and pattern noise to the total observed noise level. Toward this end, measurements of temporal noise and pattern noise versus received signal level were made.

2.4.2 Test Procedure

During the IR Camera lab tests, measurements were made that attempted to resolve the total noise level of the sensor into its temporal and pattern-induced components. Because the only signals available for measurement were composite video, the temporal noise level of a single detector element could not be directly measured. As an alternative, three indirect measurement techniques were employed. The first was to use the envelope function of the 2430 oscilloscope. This function displays the total excursion of a signal over a user-specified number of sweeps, which in this case was chosen to be 64, or

slightly over 2 seconds of data (@ 30 Hz). For a fixed input scene to the sensor, these excursions are due to random fluctuations over time. If these fluctuations are assumed to be zero-mean Gaussian distributed, then their total excursion over a reasonable length of time may be taken to represent six times the rms level (i.e., 99.7% of a Gaussian distribution is contained within +/- three standard deviations, or rms levels, from the mean). Thus, by measuring the width of the envelope from a single video line and dividing by six, one obtains an estimate of the rms temporal noise level.

The second method used for temporal noise measurement was to repeatedly digitize video frames with the FG-100 frame grabber, and observe the value of a single pixel. This method produces a time series of pixel values whose rms deviation may then be computed and converted to an equivalent voltage.

The third method also employed the FG-100. The rms deviation from a 20 line by 100 pixel region was measured as function of the number of frames averaged by the FG-100, which may be specified by the PC operator. The averaging of N frames should reduce the temporal noise variance by a factor of 1/N (i.e., reduce the rms level by a factor of 1/square root of N). In contrast, the variance due to fixed-pattern effects is not averaged out by frame integration. By analyzing measured variance versus N, the components of the total measured variance due to temporal noise and pattern noise may be inferred. (This concept is explained further in Figure 2-21.)

As discussed previously, pattern noise level is linearly proportional to the received scene flux. This dependence was quantified for each gain setting by analyzing the rms deviation over the entire FOV as a function of received irradiance. The data used in this analysis were collected during the Broadband Signal Transfer Test described in Section 2.2.

2.4.3 Test Results

The results of the pattern noise versus irradiance analysis are shown in Figure 2-19 for the four gain levels. The values of rms deviation shown in the plots were obtained by converting digital rms levels, as measured with the FG-100, into equivalent voltage units. (Note: From Figure 2-5, one digital count = 2.71 mV.) The measurements were made with a frame integration factor of 16 in order to reduce the effects of temporal noise. The degree of linearity exhibited in the plots of Figure 2-19 indicates that pattern noise dominates the total noise level at all four gains for the irradiances shown.

Because of the offset correction performed by the Reference Frame subrtraction, the measured pattern noise should be due predominantly to responsivity variations between detectors. As a result, the pattern level in any scene should be a constant fraction of the absolute mean signal. The constant of proportionality is the (normalized) rms level of the responsivity distribution across the FPA. In order to quantify this value, the measured noise levels in

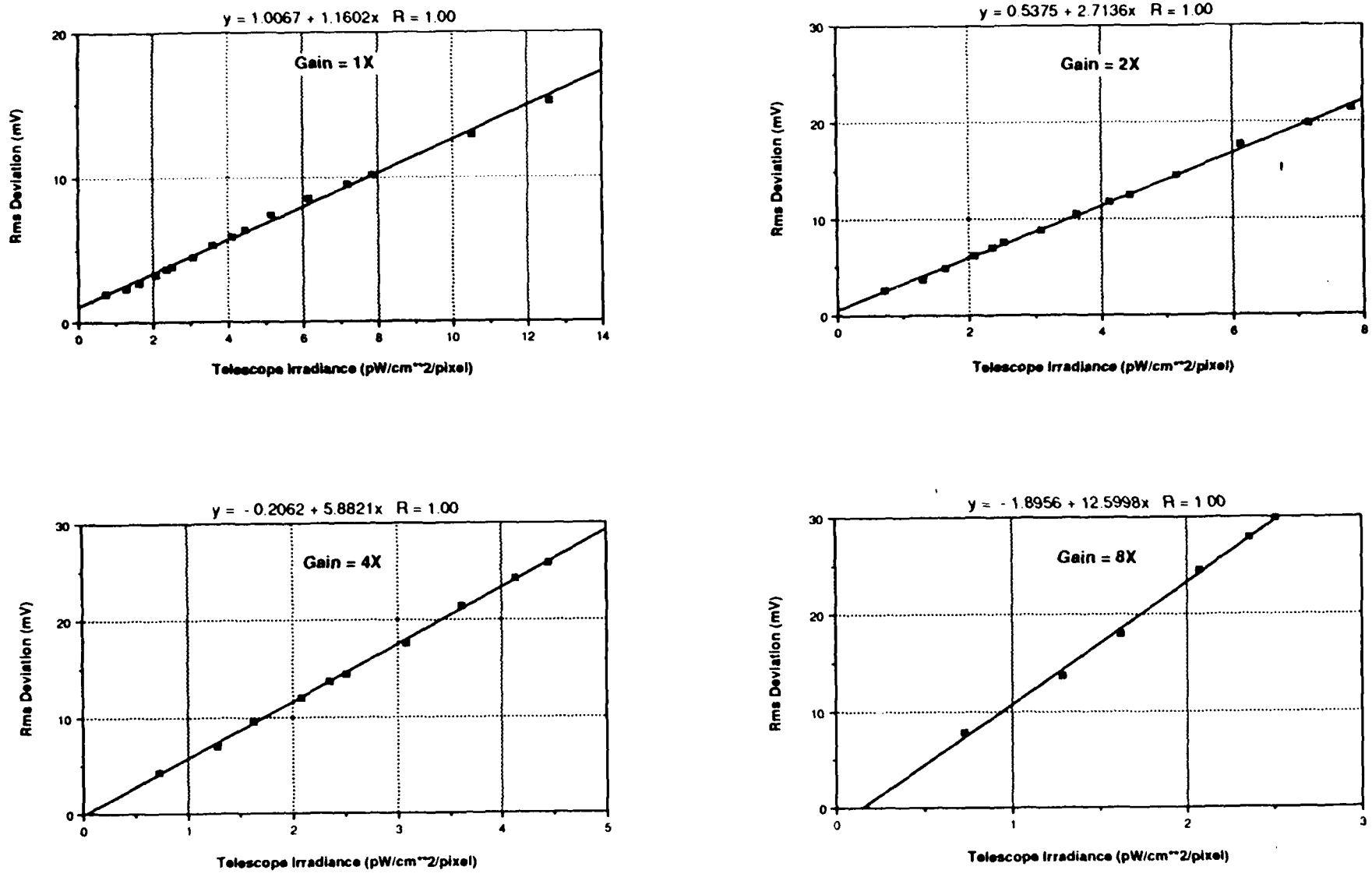

Figure 2-19. Measured Noise Level vs. Irradiance

Figure 2-19 were divided by the mean signal levels measured for the same input irradiances (Figures 2-7 through 2-10). (Actually, the mean signal levels were corrected for the different offsets associated with each gain so that zero input irradiance corresponded to zero signal out.) The results are shown in Figure 2-20 for the four gain settings. A fairly constant level of normalized deviation is observed for all four gain settings. At the lower gain levels, the normalized ratio increases for lower input irradiances. This probably reflects the influence of other noise components that dominate the relatively small pattern levels produced by low irradiances at low gains. At higher irradiances, the pattern level becomes large enough to dominate the total noise. At higher gains, this situation holds for all the irradiance levels measured. Overall, the pattern level at any gain is approximately three to four percent of the mean signal.

The results from the three methods used for temporal noise characterization are summarized in Table 2-8. With all three methods, noise levels were measured from both an ambient scene and one that was somewhat warmer. Higher noise levels were consistently obtained for the warmer scenes, which suggests that individual detectors are background limited (at least at the higher gain settings). The results obtained with the Envelope and Single-Pixel methods agree with each other quite well. The single exception is the slightly lower than expected value measured for a 61 degree C scene using the Single-Pixel method.

The results obtained from the third method, the variance versus frame integration analysis, agree less well with the other results. Figure 2-21 summarizes the basis and results of the third method. A linear regression analysis of measured variance versus 1/N yields a slope and offset that may be interpreted as the temporal and pattern variances, respectively. The square roots of these values represent the corresponding rms quantities, and these are the values shown in Table 2-8. The total rms values obtained with the third method agree well with those of the first two methods; however, this total represents both pattern and temporal effects, while the first two methods supposedly represent only the temporal component. This discrepancy suggests either the first two methods are measuring more than just temporal noise, or else the assumptions underlying the third method are incorrect. The differences between the results of the three methods are fairly minor, however, and the weight of evidence indicates the Envelope method results are probably valid. These values were therefore used in Equation 2-5 to compute Noise Equivalent quantities.

The radiometric sensitivity of the IR Camera was computed using Equation 2-5 and the noise values shown under "Method A" in Table 2-8. The results are shown in Table 2-9. For the broadband case, Noise Equivalent Irradiance (NEI) and Noise Equivalent Radiance (NER) are shown for each gain setting. The dynamic range for each gain is also shown, and was defined as the NEI divided into the maximum measurable irradiance for each gain. These maximum irradiances were defined as those producing a signal of 800 mV, the top of the electronics linear range, for all the gains except 1X. At 1X, a maximum irradiance of 15

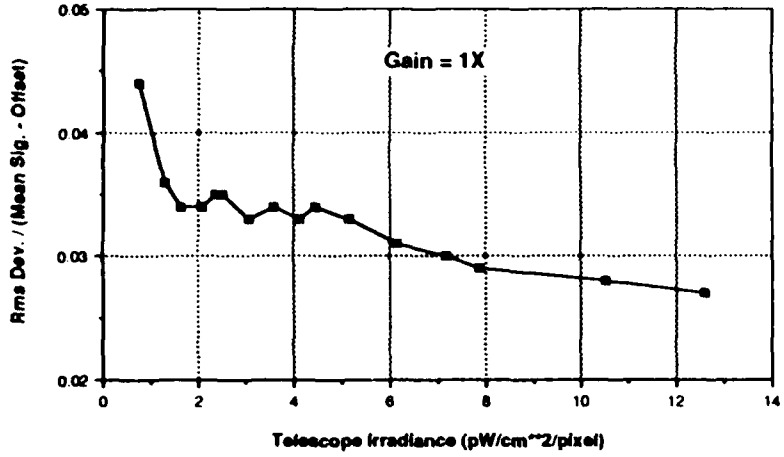

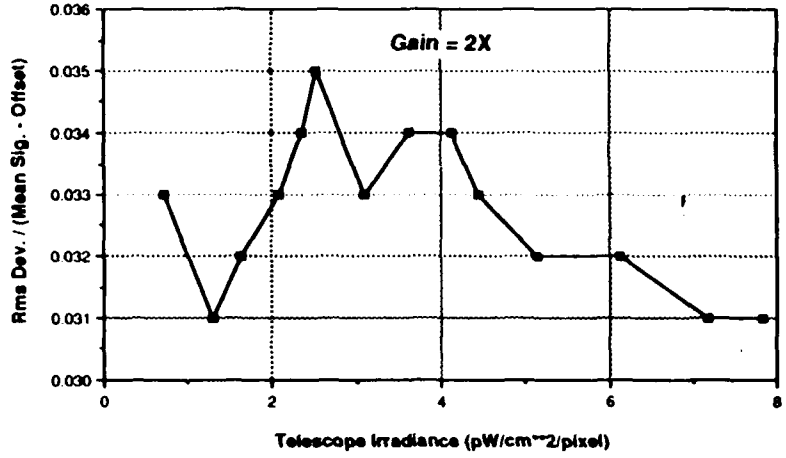

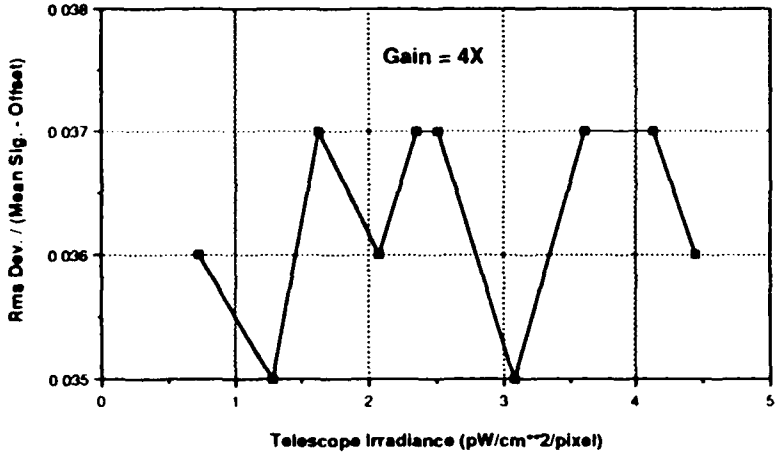

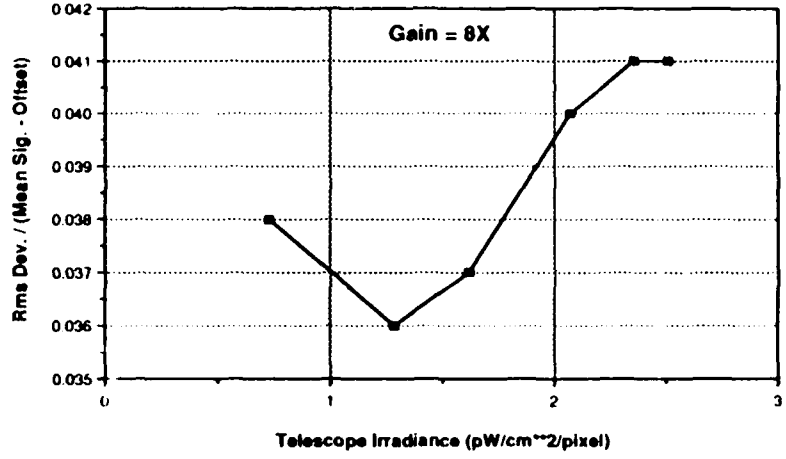

Figure 2-20. Normalized RMS Deviation vs. Irradiance

Table 2-8. Summary of Temporal Noise Measurements

Method A: Envelope measurements via 2430 oscilloscope

	RMS Noise Levels	
Gain	27 °C Scene	42 °C Scene
1X	2.5 mV	2.5 mV
2X	3.2 mV	3.4 mV
4X	4.1 mV	4.5 mV
8X	6.6 mV	7.2 mV

Method B: Single-pixel measurements via FG-100 frame grabber

Scene Temperature:	30.5 °C	61 °C	58 °C
Rms noise level:	6.4 mV	7.0 mV	7.8 mV

(Note: Measurements made @ Gain = 8X)

Method C: Linear regression of Variance vs. 1/N

	RMS Noise Levels	
	29 °C Scene	59 °C Scene
RMS (Temporal):	4.6 mV	5.5 mV
RMS (Pattern):	4.8 mV	5.8 mV
RMS (Total):	6.7 mV	8.0 mV

(Note: Measurements made @ Gain = 8X)

Define: N = number of video frames integrated for measurement
Var(total) = total measured variance (i.e., square of rms)
Var(temporal;N=1) = variance due to temporal noise @ N=1
Var(pattern) = variance due to fixed-pattern noise

Assume: 1) Frame integration reduces temporal variance by 1/N
2) Temporal and pattern noises are independent, so that
Var(total) = Var(temporal) + Var(pattern)

Then, **Var(total) = (1/N)*Var(temporal;N=1) + Var(pattern)**

and Var(temporal,N=1) and Var(pattern) may be found via linear regression of measured Var(total) versus 1/N

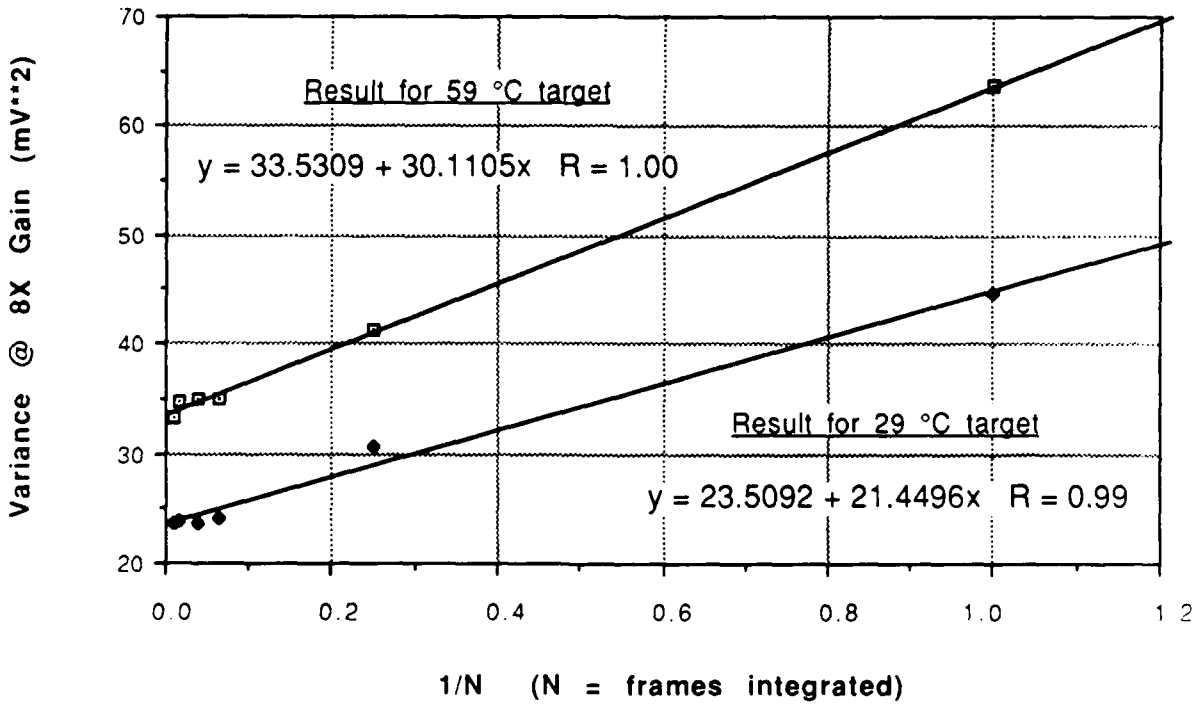

Figure 2-21. Noise Level vs. Frame Integration

Table 2-9. Summary of IR Camera Sensitivity Measures

- Broadband Results:

Gain	RMS Noise	Responsivity mV/(W/cm**2)	NEI Watts/cm**2	NER Watts/cm**2/sr	Dynamic Range *
1X	2.5 mV	4.46 E+13	5.6 E-14	7.0 E-5	270:1
2X	3.2 mV	8.78 E+13	3.6 E-14	4.6 E-5	240:1
4X	4.1 mV	1.59 E+14	2.6 E-14	3.2 E-5	190:1
8X	6.6 mV	2.93 E+14	2.3 E-14	2.8 E-5	120:1

(* Single-frame values; total dynamic range over all gain levels is 650:1)

- Spectral Sub-Band Results:

  - Values shown are for Gain = 8X, and an rms noise level of 6.6 mV

Sub-Band Designation	Responsivity mV/(W/cm**2/sr/μm)	NESR W/cm**2/sr/μm	NER W/cm**2 sr
RED (2.04 μm)	5.26 E+5	1.3 E-5	1.1 E-6
	3.26 E+5	2.1 E-5	1.8 E-6
BLUE (2.805 μm)	3.41 E+5	2.0 E-5	5.0 E-6
YELLOW (4.484 μm)	1.65 E+4	4.1 E-4	3.0 E-5

picowatts per square centimeter was used (cf., Figure 2-7).

The lower portion of Table 2-9 contains values of Noise Equivalent Spectral Radiance (NESR) and NER for the three spectral sub-bands. The two quantities differ only by the bandwidths of the spectral filters. Two values are shown for the Red band because of the observed non-linearities in repsonsivity (cf., Figure 2-16). The two values shown correspond to input irradiances of 0.5 and 1.0 mW/(cm**2 sr um), respectively.

The fact that system sensitivity depends on gain level, as is indicated by the results of Table 2-9, implies the sensor is not detector-noise-limited, and therefore not truly background-limited. If the limiting noise was from the detectors (e.g., due to background or readout noise), responsivity and noise level would be affected equally by a gain change, and their ratio would therefor remain constant. The measured sensitivity does not, on the other hand, vary with gain at the same rate as does responsivity. This situation would occur if the noise level was predominantly gain-independent, and therefore independent of the detector signals. It appears, therefore, that the sensor is nearly background-limited, and becomes more closely so at the higher gain levels.

2.5 COLD SENSOR TEST

2.5.1 Discussion/Test Purpose

There is a large mismatch between the f-number of the telescope, which is f/10, and that of the dewar/cold-shield, which is f/1.6. As a result, of the total (uncooled) cone of radiation received by the detector, only 1/39th of that cone contains the scene energy collected by the telescope. (Note: The factor of 39 represents the square of the f-number ratio.) The remaining 38/39ths contains radiation from the telescope housing itself, which is at the temperature of the ambient environment. This component represents a relatively large, constant flux level on the FPA, independent of the background scene temperature. Indeed, a background temperature approaching 200 degrees Celsius is required before the resulting flux on the detectors exceeds that from the telescope at room temperature.

The f-number mismatch has several deleterious effects on sensor performance due to the large background level represented by the telescope thermal emission. For example, the large background may represent the principal source of temporal noise. As stated in Section 2.4, the sensor appears to be nearly background limited (at least at 8X gain) in that increasing the scene temperature increases the temporal noise level (cf., Table 2-8). This situation, however, may only be due to the very high background level of the telescope. If this level were reduced by cooling the telescope, the sensor might not be BLIP limited, but its total noise level (at the higher gains) would be reduced. Because the responsivity would not change, a net gain in sensitivity would result.

Another benefit of reducing the telescope background contribution would be an increase in dynamic range, because the detector charge wells would no longer have to accomodate as many background-produced electrons. Thus, higher scene irradiances could be viewed before saturation occurred. The situation might improve enough to permit removal of the dewar neutral density filter. This change would improve the system sensitivity by as much as a factor of two.

The large telescope background also affects the Reference Frame. Consider, for example, a Reference Frame stored with the clear setting of the spectral filter wheel (i.e., the broadband setting). This Reference Frame will represent a large signal from the detectors, due to the telescope, even if a very cold external background is viewed. At any of the narrow sub-band settings, however, a much smaller fraction of the total telescope emission reaches the detector, and so, the total signal (for the same scene) is also much smaller. When the large broadband Reference Frame is subtracted from this signal, the latter will be lost to black video saturation unless a very large Black Level offset is used to compensate. Even the maximum Black Level offset may not be sufficient in some cases. The converse situation is if the Reference Frame is stored with one of the sub-band filter settings. If the scene is then viewed with the broadband setting, the large signal produced by the telescope will produce white video saturation of the scene information. The telescope background level thus precludes the use of a single Reference Frame with all four filter wheel settings. As a result, near-simultaneous data collection with all four filter settings, which is the purpose of the rotating filter wheel, cannot be accomplished.

The phenomena described above are hypothetical consequences of the f-number mismatch; their existence has never been confirmed experimentally. An attempt to do so was made by cooling the telescope and assessing the change in sensor behavior. The test procedure and results are described below.

2.5.2 Test Procedure

The IR Camera sensor head was cooled by placing it inside a large refrigerator, whose temperature was approximately 40 degrees Farenheit (4 deg. C), for a period of 14 hours. The head was then removed, connected to the the rest of the system, and used to collect data. Two tests were performed, although only one of these yielded useful data. In the first test, a Reference Frame of a cooled object (the same wood plate used during the signal transfer tests) was stored with the filter wheel set at the Yellow sub-band position. Then, with the telescope lens cap on, the signal level for each of the four filter wheel positions was measured. The lens cap consists of a relatively thin sheet of plastic, and was essentially at the ambient room temperature of 26 degrees C. The same measurements were repeated after the sensor had warmed to nearly room temperature. The change in signal levels observed at the various filter settings permitted assessment of the Reference Frame effect described in Section 2.5.1.

The second test consisted of signal measurements at the four filter wheel settings while viewing the laboratory blackbody. The intent was to repeat a test point from the signal transfer tests in order to assess changes in the absolute signal level(s) produced by a constant blackbody temperature. The measurements were repeated at regular intervals in time as the sensor head warmed toward room temperature. A Reference Frame was stored before each signal measurement. Any changes in absolute signal level could then be attributed to the Reference Frame signal changing with telescope temperature. Although this effect is closely related to that addressed by the first test, the second test results would have been more directly related to the effect of telescope temperature upon the calibration of each spectral band.

Unfortunately, the data collected in second test was rendered meaningless due to moisture condensation on the telescope mirrors, which resulted from the sensor temperature being below the ambient dew point. The condensation reduced the effective optics transmission considerably, apparently to zero in some of the sub-bands. A layer of moisture was clearly visible on the primary telescope mirror; however, even after it had evaporated, the sensor repsonse was still substantially attenuated, presumably due to residual moisture on the spectral filters and/or other interior optics. Eventually, the full response was observed, but not until the entire telescope had warmed to nearly room temperature. Consequently, the data collected in the second test were determined to be of little value and are not reported. The data from the first test were unaffected by condensation because: 1) the telescope interior had not yet been sufficiently exposed to the ambient during the cooled sensor measurements, and 2) the telescope had dried by the time of the ambient sensor measurements.

2.5.3 Test Results

The results of the first test are summarized in Table 2-10. The signal levels shown are those of the telescope covered with the ambient lens cap. The change in telescope temperature between the two sets of data was approximately 20 degrees Celsius. The Reference Frame used for all four filter settings was collected with the Yellow sub-band.

Table 2-10. Lens Cap Signals with Cooled and Ambient Telescope

Filter Setting:	Broadband	Red	Blue	Yellow
Cooled telescope:	443 mV	330 mV	106 mV	105 mV
Ambient telescope:	1030 mV *	792 mV	157 mV	120 mV
Difference:	587 mV *	462 mV	51 mV	15 mV

(* limited by output electronics)

Very large signal changes were observed for the Broadband and Red filter settings, while smaller changes occured in the other two sub-bands. Because the Yellow band was used as the source of the Reference Frame in each measurement, no signal change should have been observed for that sub-band. The 15 mV difference that was observed is probably due to dc drift in the sensor output (an effect that was observed in all the lab tests). As indicated in Table 2-10, the Broadband signal with the ambient telescope was beyond the range of the sensor output electronics. This illustrates the Reference Frame effect described in Section 2.5.1. With the telescope cooled only 20 degrees C below ambient, Table 2-10 shows that a single Reference Frame permits unsaturated signals at all four filter settings.

The large difference between the signal changes observed in the Red and Blue sub-bands is surprising. Ambient temperatures contribute very little energy to the spectral regions represented by these two bands (2.04 and 2.805 um, respectively), and so a rather small dependence on telescope temperature would have been expected. The very large change in the Red sub-band suggests that its spectral filter transmits significant energy at longer wavelengths. This effect would also explain the higher than predicted responsivity of this sub-band (cf., Section 2.3).

Overall, the results of the Cold Sensor Test should probably be interpreted only qualitatively. Nevertheless, they show a significant dependence of sensor behavior upon telescope temperature. This effect warrants additional consideration, as discussed in Section 3.0.

2.6 RESOLUTION/FOCUS TEST

2.6.1 Purpose

The purpose of this test was to measure the effective spatial resolution of the IR Camera at four different points in the field of view, as well as assess whether or not the telescope was properly focussed.

2.6.2 Test Procedure

The sensor resolution was assessed by imaging a very thin wire (.001" dia.) and measuring the resulting line-spread function (LSF) on the 2430 digital oscilloscope. The image of the wire at the detector focal plane was approximately 20 um, as compared with the 40 um vertical by 80 um horizontal dimensions of an individual detector element. The wire was oriented vertically for all of the measurements, and so the results are indicative of the horizontal resolution only. The horizontal readout of the FPA provides an effective scan over the wire image to produce the LSF. Measurement of the vertical resolution would have required discrete measurements of a single detector output as the wire image was physically translated across it. The mechanical tolerances for performing such a measurement would have required wire translations on the order of a

few micrometers. This is well beyond the capability of the laboratory vertical translator, which has a precision of 0.001 inches (25 micrometers).

The focus of the sensor telescope, which is supposed to be set at infinity, was assessed by measuring the plane of best sensor focus with respect to the known collimator focal length of 100.25 inches. If the telescope is truly focussed at infinity, its plane of best focus should be 100.25 inches from collimator mirror surface. Any other position indicates focus at a point other than infinity, whose position may be estimated by the thin lens equation

$$(1 / D\_obj) + (1 / D\_img) = 1 / f \qquad (2\text{-}6)$$

where D_obj = object distance, D_img = image distance, and f = focal length (nominally, 80 inches for the sensor telescope).

2.6.3 Test Results

The plane of best focus for the telescope was found to lie at 99.75 inches from the collimator surface, or 0.5 inches inside the plane of infinity focus. The corresponding longitudinal offset (i.e., along the optical axis) between the FPA and the telescope focal length is given approximately by the measured 0.5 inch offset times the square of the telescope/collimator focal length ratio. Thus, the FPA is displaced (0.5 inches) (80/100)**2 = 0.32 inches beyond the focal point of the telescope. For f = 80 inches, and D_img = 80.32 inches, Equation 2-6 gives D_obj = 1670 feet as the object distance focussed onto the detectors. For a properly adjusted telescope, the minimum focal distance is supposed to be approximately five miles; thus, a significant telescope alignment problem appears to exist.

It should be noted that the telescope focus problem in no way compromises the calibration data collected in the other lab tests. This is because a field-filling, extended blackbody source was used, and so the loss of signal energy due to misfocus on any detector element was compensated for by the spread of energy from adjacent regions.

The line spread-function measurements were made with the wire source located at 99.75 inches from the collimator, i.e., in the plane of best focus. Five points in the field of view were measured; the measurement locations are indicated in Figure 2-22a. Figure 2-22b shows the typical LSF shape as measured on the 2430 scope. The responses of the individual elements were clearly discernable as shown in the figure. Note the characteristic decaying exponential form of each detector's output. Figure 2-22c shows the 25 um by 50 um active region of each 40 um by 80 um detector. Adjacent detector elements are virtually contiguous so that the center-to-center spacings of the active regions (i.e., the effective pitch) are equal to the full element sizes. The gaps between active areas are on the order of the 20 um image size of the wire source. During the test, it was possible

via subtle shifts of the wire position to move the response peak from one element to its immediate neighbor. A null region between the elements was easily demonstrated.

At each of the five points shown in Figure 2-22a, the 50% and 20% response widths of the LSF were measured. The results are summarized in Table 2-11. The widths are given in units of both time and equivalent object space angle. The measured angular scan rate that relates time to angle is shown in the table. The values in Table 2-11 show that the resolution is essentially independent of position in the FOV. Note the apparently much better resolution at point C. These results are are believed to be an artifact of the detector geometry illustrated in Figure 2-22c. A relatively large peak repsonse voltage was observed at point C. This response was probably the result of the wire image falling squarely on the active region of the central detector element (cf., Figure 2-22b). At the other four points, the alignment was probably less optimal, resulting in smaller peak responses and thus, wider response widths at the 50% and 20% points. These differences are not believed to represent real differences in resolution across the FOV. As shown in Table 2-11, a discernible response to the wire image was observed over a width of seven to eight detectors; however, the response falls off sharply outside the central three elements. The measured spread functions may be assumed to be circularly symmentric, and thus, also representative of the vertical angular resolution. Note that vertically, however, twice as many detector elements lie under the spread function as for the horizontal case, due to the element geometry shown in Figure 2-22c.

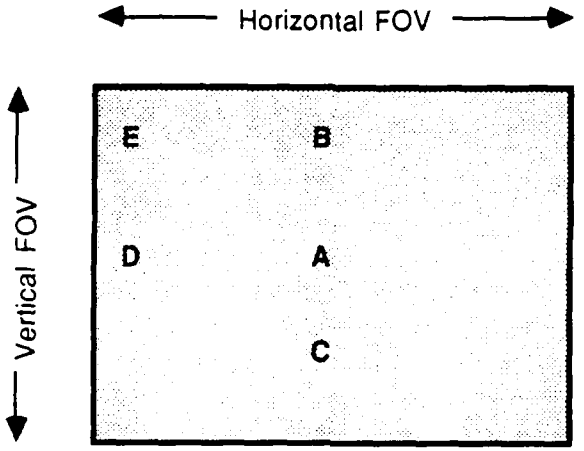

(a) Measurement points within FOV

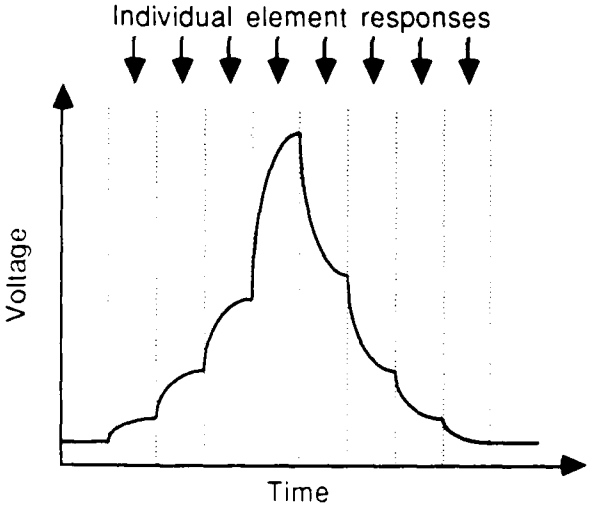

(b) Typical LSF response

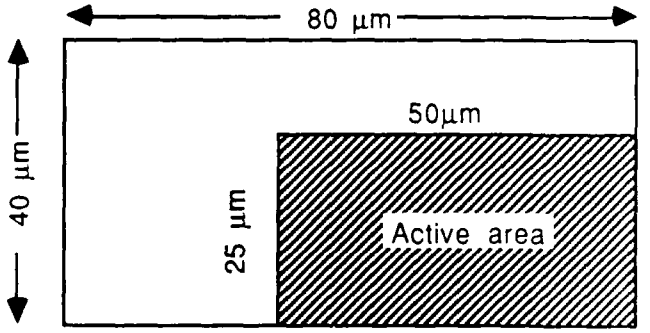

(c) Detector size; active region

Figure 2-22. Line Spread Function Measurements

Table 2-11. Summary of Line Spread Measurements

	LSF 50 % Width		LSF 20 % Width	
Point	Time	Angle *	Time	Angle *
A	0.59 μsec	71 μrad	1.0 μsec	120 μrad
B	0.53 μsec	64 μrad	0.79 μsec	95 μrad
C	0.39 μsec	44 μrad	0.74 μsec	89 μrad
D	0.60 μsec	73 μrad	0.85 μsec	103 μrad
E	0.60 μsec	73 μrad	0.85 μsec	103 μrad

(* Equivalent angles calculated via measured scan rate of 120 μrad/μsec)

100 % of LSF contained within 7-8 detector elements (~ 300 μrad)

3.0

SUMMARY AND RECOMMENDATIONS

In this section, the major test results are summarized and recommendations for potential system improvements are given.

3.1 SUMMARY OF TEST RESULTS

The four test objectives identified in Section 1.0 were met. Signal transfer functions were measured using a calibrated, temperature-controllable blackbody source. The sensor exhibited linear response to within a few percent over its dynamic range. A procedure for radiometric calibration of data collected with the IR Camera was defined and appears in Appendix B. The procedure includes a gain-dependent correction for Black Level setting, and is applicable to data collected in any of the sensor's four spectral bands.

Radiometric sensitivity in each of the four spectral bands (i.e., broadband and three sub-bands) was defined; the values are summarized in Table 2-7. The Noise Equivalent Radiance at the broadband filter setting and the Noise Equivalent Spectral Radiances for each of the sub-bands were found to be on the order of 1.E-5 or larger. These values are at least two orders of magnitude larger than the currently defined requirement of 1.E-7 for MWIR sensing of plume signatures. Thus, system sensitivity is an issue that must be addressed if the sensor is to remain a useful data collection asset for upcoming missions.

The sensor telescope was found to be focussed at an object distance of roughly 1700 feet instead of the specified focus at infinity. Severe mis-focus occurs on objects that are effectively at infinity, e.g., mission targets. Proper alignment of the telescope is therefore required before the next sensor deployment against mission targets. For focussed imagery, the effective horizontal spatial resolution of the system, as defined by its line-spread function, was found to be roughly 75 to 100 microradians. For comparison, the diffraction limit of the 20 cm telescope aperture is around 25 microradians at 5 micrometers wavelength. The measured resolution is within the current requirement for plume sensing.

As discussed in Section 2.5.1, the f-number mismatch between the detector cold-shield and the telescope was hypothesized to produce a large background flux on the detector from the telescope itself. This theory was apparently confirmed by measurements made on the sensor after cooling the telescope by roughly 20 degrees Celsius. Significant differences were observed in the offset correction that is applied to the Corrected Video channel via the Reference Frame. It was found that with the telescope at temperatures near 300 Kelvin, the rotating filter wheel cannot be used to gather useful near-

simultaneous data in the four spectral bands. The lab tests indicated, however, that this mode of collection could be used successfully if the telescope were cooled to approximately 275 Kelvin or colder.

In the course of the tests, two anomalous aspects of the sensor's behavior were identified. The first was the occurrence of random dc drifts in the output video signal. The magnitudes of these drifts were relatively small--on the order of 10 to 15 millivolts. They were observed to occur at irregular intervals. Sometimes the dc level changed gradually over a period of several seconds, while at other times it jumped rather abruptly. The drifts were more prevalent within the first hour or two after the system was powered up, but were also observed after many hours of operation.

The second anomaly was the unusually strong response of the Red spectral sub-band, which is centered at 2.04 micrometers. Particularly based on the results of the Cold Sensor Test (Section 2.5), there is reason to suspect that the Red band spectral filter has signficant transmission at wavelengths longer than its primary passband, but still within the response range of the detector.

3.2 RECOMMENDATIONS FOR SENSOR IMPROVEMENT

Based on the test results reported above, a list of seven recommendations for potential system improvements has been formulated. The recommendations are presented in order of approximate cost, although cost figures for each have not been provided. It is not not expected that all seven items will be adopted; rather, they are intended to represent a range of possible alternatives for improving the system.

1. System Noise Analysis: Since the measured system sensitivity is significantly worse than required for many applications, several of the recommendations address the issue of sensitivity improvement. One of the easier approaches to increasing sensitivity is to ensure that the electronics are contributing no more noise than absolutely necessary. No information was provided to ERIM regarding system electronics bandwidths and their relation to the information content of the focal plane array output. It is conceivable, however, that standard video circuits, with bandwidths of four to five megahertz, are present in the signal chain. These bandwidths would be nearly twice that required by the 160 elements per video line, and therefore would introduce substantial high-frequency noise unnecesarily. An analysis of this situation, if one has not already been performed, should be the first step toward improving the system sensitivity.

2. Spectral Measurements: If spectrally accurate calibration results are critical to supporting future missions, then the spectral response of the IR Camera as a whole, as well as the spectral transmission characteristics of the sub-band filters, should be measured. The

sensor spectral response had been requested as a part of the laboratory characterization described in this report; however, the time and cost required for ERIM to make such a measurement were beyond the schedule and funding limits of the current program. A crude assessment of the sensor spectral response was attempted based on the sub-band signal transfer data. The results raised enough questions to suggest that more precise spectrometric measurements are needed, particularly to identify if the Red band filter is permitting out-of-band radiation to reach the detector.

3. Assessment of Random DC Drift: Depending on the requirements for calibration accuracy, the dc drift problem identified during the lab tests may represent a significant source of error. The problem is more severe at low gains, since a fixed drift of, say, 10 mV represents a larger error in calibrated irradiance. If the levels of error due to drift are deemed significant, then diagnosis and correction (if possible) of the drift problem is warranted.

4. Digitally-Based Calibration: The present analog-based data collection and calibration scheme does not permit the increased radiometric accuracy and effective sensitivity that a digitally-based reduction and calibration procedure could provide. The principal benefit of the digital approach is that pixel-by-pixel corrections can be formulated to account for effects such as pattern noise and vignetting. Figure 2-19 shows that for significant scene flux levels, responsivity pattern noise dominates the system temporal noise. As a result, the measured NER/NESR values--which are already inadequate for many applications--will not be effectively realized unless the individual detector responses are accounted for.

5. Cooled Telescope: As the results of Section 2.5 indicate, if data must be collected with the filter wheel rotating, then the telescope must be cooled to approximately 275 Kelvin or less. For airborne data collection, this requirement should be fairly easy (in principle) to meet by exposing the sensor head to the external air temperature. To do this will, of course, require significant modification of the sensor/airframe mechanical interface. Before such an effort is attempted, it would be prudent to repeat and expand the Cold Sensor Test under more controlled circumstances (e.g., avoid the condensation problem encounter in the ERIM lab test). As discussed in Section 2.5.1, a number of performance benefits may accrue from cooling the telescope to the proper temperature.

6. Obtain a New Telescope: The present system telescope, by virtue of its high f-number relative to the detector cold-shield, is a major cause of the relatively poor system sensitivity, as well as the background flux problem considered in the previous recommendation. It is apparent that the present telescope design is a compromise between spatial resolution requirements (which dictate the two meter focal length) and cost (which limits the aperture to the present 20 cm

figure). The penalty paid in this compromise is, however, a degradation in sensitivity by roughly a factor of 40 (assuming a non-background-limited condition, which would be the case if the telescope emission were reduced). If the two meter focal length had to be retained, a matched telescope (i.e., one that was f/1.6) would have to have a 1.25 meter aperture--a practical impossibility from a budgetary standpoint. There should be some middle ground, however, between that impractical alternative and the present situation. For example, if the IFOV could be allowed to increase by 50% (i.e., reduce the focal length from 2.0 to 1.3 meters) and the aperture diameter doubled to 40 cm, the improvement in sensitivity would be nearly an order of magnitude (as would the improvement in the telescope background problem). The requirements for spatial resolution should be assessed in relation to those for radiometric sensitivity in order to identify a suitable compromise and an appropriate telescope design.

7. Direct Digital Recording: The benefits of digital processing described under item #5 above would be most fully realized if the detector signals were stored digitally rather than on analog video tape. Such a system would facilitate the most accurate data reduction and calibration, as well as improve the data utility (e.g., directly compatible with computer models) and processing throughput. The system sensitivity would also be enhanced through the elimination of noise-inducing analog video electronics. The digital recording approach, however, is relatively expensive and would require a significant period of time to implement. The long-term utility of the sensor would have to be confirmed before such a modification would be justified.

Appendix A

Raw Laboratory Test Data

Table A-1. Black Level Response Test Data

Black Level	V_active(8X)	V_active(4X)	V_active(2X)	V_active(1X)	V_dead
0.500	59.4	61.8	62.8	64.4	64.4
0.600	61.8	66.	68.4	70.6	64.8
0.700	66.8	72.8	76.	78.2	65.8
0.800	75.6	83.2	86.4	88.6	66.8
0.900	99.	101.2	99.8	100.	67.2
1.000	112.6	114.6	113.4	113.	68.6
1.100	125.8	127.	125.	124.2	69.4
1.200	141.6	140.	136.8	135.	69.6
1.300	155.	152.	149.	147.5	70.5
1.400	168.5	166.	161.	159.5	71.
1.500	181.5	178.	173.5	170.5	72.5
4.000	475.	470.	463.	462.	100.
6.500	773.	764.	759.	755.	136.
7.000	842.	834.	826.	826.	146.
8.000	960.	950.	946.	938.	160.
9.000	1042.	1040.	1034.	1034.	172.
10.000	1042.	1042.	1042.	1042.	184.

Black Level = Black Level control dial setting

V_active(g) = measured voltage [millivolts above porch] of active video line for gain setting "g"

V_dead = measured voltage [mV above porch] of "dead" video lines

Table A-2. Broadband Signal Transfer Test Data

E[pW/cm**2]	V_peak (1X)	V_peak (2X)	V_peak (4X)	V_peak (8X)	Dig Val (1X)
0.728	106	121	154	210	1.85
1.286	119	160	238	382	9.1
1.622	134	191	298	500	14.2
2.073	160	232	378	650	20.35
2.358	171	257	419	730	23.86
2.511	177	268	443	780	25.64
3.082	202	323	571		35.41
3.610	224	364	640		42.58
4.128	249	411	735		50.8
4.449	261	439	790		55.36
5.150	298	516			69.78
6.136	350	620			88.28
7.177	393	716			104.02
7.839	426	784			115.22
10.520	552				158.6
12.580	651				195.5
14.740	733				226.6
16.700	796				248.5
20.940	850				255

E[pW/cm**2] = calculated band irradiance (2.0-5.5 um) of laboratory blackbody in picowatts per square centimeter per detector

V_peak(g) = measured peak voltage [mV above porch] at center of field of view (measured via Tektronix 2430) for gain setting "g"

Dig Val(g) = average digital value over entire FOV for gain "g"

Voltage Level = voltage in mV above porch used to characterize the transfer function of the FG-100 frame grabber (i.e., the relationship between voltage in and digital counts)

Digital Level = the observed digital level output by the FG-100 when "Voltage Level" was input (cf., Figure 2-5)

V_dig(g) = equivalent voltage level [mV above porch] of Dig Val(g) as defined by the FG-100 signal transfer characteristic

Lin_Dev(g) = calculated deviation from linearity in percent for gain "g"

Table A-2. (con'd)

Dig Val (2X)	Dig Val (4X)	Dig Val (8X)	Voltage Level	Digital Level	V_dig (1X)
7.17	18.11	36.77	99.2	0.84	104.410
22.08	48.46	97.65	127.8	10.57	124.043
32.64	69.98	136.35	168.	25.	137.854
45.72	96.83	187.75	231.	47.97	154.508
52.85	110.9	213.26	241.	51.39	164.013
56.51	118.29	228.9	298.	74.39	168.833
77.21	160.15		354.	94.21	195.290
91.6	184.58		473.	136.85	214.707
107.95	217.78		587.	180.72	236.966
117.	235.86		708.	224.77	249.315
143.1			757.	242.9	288.364
180.39					338.462
212.6					381.086
235.59					411.416
					528.889
					628.814
					713.033
					772.338
					789.940

V_dig (2X)	V_dig (4X)	V_dig (8X)	Lin_Dev(1X)	LIn_Dev(2X)	Lin_Dev(4X)	LIn_Dev(8X)
118.816	148.442	198.973	12.300	14.600	2.600	-1.500
159.193	230.630	363.836	5.200	4.300	-1.300	-0.550
187.789	288.906	468.636	3.700	3.100	0.564	0.889
223.210	361.616	607.827	0.971	0.651	0.664	1.800
242.518	399.717	676.908	-1.000	-1.700	-1.200	-0.544
252.429	419.729	719.261	-2.200	-3.000	-2.200	-0.865
308.485	533.086		-1.400	-0.602	2.500	
347.453	599.243		-3.100	-2.600	-0.858	
391.729	689.148		-3.200	-2.600	0.304	
416.236	738.109		-3.800	-3.300	-0.022	
486.915			-0.697	-1.000		
587.896			1.200	1.600		
675.121			0.054	0.784		
737.378			0.240	1.300		
			-0.232			
			1.100			
			-0.762			
			-4.200			
			-20.600			

Table A-3. Spectral Sub-Bands Signal Transfer Test Data

Radiance_Red	Volts_Red	Radiance_Blue	Volts_Blue	Rad_Yellow	Volts_Yellow
0.0033	135.7	0.065	122.	3.277	153.
0.0059	150.3	0.100	132.	7.303	214.
0.019	167.5	0.233	170.	8.995	229.
0.141	272.	0.822	366.	11.000	273.
0.176	311.	1.142	478.	14.000	330.
0.271	387.	1.557	620.	18.000	422.
0.462	484.	2.287	880.	22.000	454.
0.853	675.			32.000	615.
1.239	796.				

Radiance_Red = spectral radiance [milliwatts per square centimeter per steradian per micrometer] calculated over the RED spectral sub-band (2.04 um)

Volts_Red = measured voltage [mV above porch] at center of FOV for the RED sub-band @ gain 8X

Radiance_Blue = spectral radiance [mW/(cm**2 sr um)] in the BLUE sub-band (2.804 um)

Volts_Blue = measured voltage in the BLUE sub-band @ gain 8X

Rad_Yellow = spectral radiance [mW/(cm**2 sr um)] in the YELLOW sub-band (4.484 um)

Volts_Yellow = measured voltage in the YELLOW sub-band @ gain 8X

Table A-4. RMS Noise Level vs. Irradiance Data

E[pW/cm**2]	Sigma (1X)	Sigma (2X)	Sigma (4X)	Sigma (8X)
0.728	.71	.96	1.59	2.92
1.286	.84	1.36	2.59	5.05
1.622	.97	1.77	3.52	6.63
2.073	1.18	2.27	4.42	9.08
2.358	1.32	2.57	5.05	10.31
2.511	1.40	2.77	5.32	11.03
3.082	1.66	3.25	6.49	
3.610	1.96	3.90	7.89	
4.128	2.17	4.38	8.94	
4.449	2.35	4.66	9.53	
5.150	2.74	5.36		
6.136	3.17	6.54		
7.177	3.52	7.32		
7.839	3.78	7.93		
10.520	4.79			
12.580	5.63			
14.740	5.61			
16.700	5.39			
20.940	---			

E[pW/cm**2] = calculated blackbody irradiance [picowatts/square centimeter]

Sigma(g) = measured digital standard deviation over entire FOV @ gain "g"

Table A-5. Variance vs. Frame Integration Data

N	1/N	Dig_rms_hot	Dig_rms_amb	Volt_rms_hot	Volt_rms_amb	Variance_hot	Variance_amb
1	1.000	2.946	2.464	7.977	6.678	63.633	44.596
4	0.250	2.369	2.041	6.415	5.531	41.152	30.592
16	0.063	2.182	1.816	5.908	4.921	34.904	24.216
25	0.040	2.187	1.796	5.922	4.867	35.070	23.688
64	0.016	2.173	1.807	5.884	4.897	34.621	23.981
100	0.010	2.132	1.791	5.773	4.854	33.328	23.561

N = number of frames averaged to measure rms noise level

1/N = reciprocal of "N"

Dig_rms_hot = measured digital standard deviation for a 59 degree C target

Dig_rms_amb = measured digital standard deviation for a 29 degree C target

Volt_rms_hot(amb)= equivalent rms voltage level corresponding to Dig_rms_hot(amb)

Variance_hot = squared value of Volt_rms_hot

Variance_amb = squared value of Volt_rms_amb

Appendix B

Calibration Procedure for IR Camera Corrected Video Data

Calibration Procedure for IR Camera Corrected Video Data

The following procedure may be used to convert signal levels from the *Corrected Video* channel of the ARGUS IR Camera into Irradiance (for Broadband signals) or Spectral Radiance (for Sub-Band signals):

Step 1. Measure Signal Level

Measure voltage level, V_{meas} , in millivolts with respect to porch level; apply corrections as necessary to convert measured value to equivalent voltage out of sensor, V_{sensor}

Step 2. Apply Black Level Correction (BLC)

Define BL(mission) as the Black Level dial setting (0.00 to 10.00) used during data collection. Calculate the Black Level corrected voltage, V_{BLC}, from V_{sensor} via the following equation:

$$V_{BLC} = V_{sensor} + A(g) * [\ BL(lab) - BL(mission)\ ] - Dev(g,filter)$$

where, BL(lab) = 0.80 for Broadband data
= 1.20 for Sub-Band data

and A(g), Dev(g,filter) are defined in the table below for gain level "g" and filter= Broadband or Sub-Band

Gain level (g):	1X	2X	4X	8X	
A(g):	117.1	121.5	127.9	138.8	mV/dial unit
Dev(g,Broadband):	0.2	1.9	5.5	9.5	mV
Dev(g,Sub-Band):	0.0	0.0	0.0	0.0	mV

Step 3. Convert V_{BLC} to Radiometric Units

Convert V_{BLC} to the appropriate radiometric quantity at the telescope:

a) Irradiance E_{tel} (pW/cm**2/pixel) for Broadband data

b) Spectral Radiance $L_{\lambda,tel}$ [mw/(cm**2 sr μm)] for Sub_Band data

a) Broadband Data:

$$E_{tel} = \frac{V_{BLC} - V_o(g)}{R(g)}$$

where R(g) and $V_o(g)$ are given in the table below.

Gain (g):	1X	2X	4X	8X	
R(g):	44.64	87.79	159.5	293.6	mV/(pW·cm**2)
$V_o(g)$:	60.5	39.8	28.5	-11.7	mV

a) Sub-Band Data (applicable to 8X Gain only):

RED Band: $L_{\lambda,tel} = -0.123 + 8.453E\text{-}4 \cdot V_{BLC} + 1.009E\text{-}8 \cdot V_{BLC}^2 + 1.345E\text{-}9 \cdot V_{BLC}^3$

BLUE Band: $L_{\lambda,tel} = (V_{BLC} - 93.4) / 340.72$

YELLOW Band: $L_{\lambda,tel} = (V_{BLC} - 96.0) / 16.48$

Step 4. Correct for Germanium Window Transmission

Divide E_{tel} or $L_{\lambda,tel}$ by 0.98, the measured Ge window transmission, to convert them to the equivalent quantities outside the window